Chemical Engineering Journal 466 (2023) 143197

Contents lists available at ScienceDirect

Chemical Engineering Journal

journal homepage: www.elsevier.com/locate/cej

Review

Recent advances and perspectives of electrode materials for emerging ammonium-ion storage: From mechanistic insights to practical applications

Wanying Zheng [a], Xi Hu [a], Mengcheng Wu [a], Lingyun Chen [a,*], Shaowei Chen [b,*]

[a] Department of Applied Chemistry, School of Chemistry and Chemical Engineering, Chongqing University, Chongqing 401331, PR China
[b] Department of Chemistry and Biochemistry, University of California, Santa Cruz, 1156 High Street, CA 95060, USA

ARTICLE INFO

Keywords:
Ammonium-ion storage
Cathode materials
Anode materials
Storage mechanism
Hydrogen bond

ABSTRACT

The aggravation of energy and environmental issues forces people to develop sustainable energy storage technologies. In recent years, emerging ammonium-ion storage has been considered a promising energy storage competitor because of NH_4^+ ions as charge carriers with merits of abundant resources, inherent safety, fast diffusion capability and unique storage mechanism. However, the development of NH_4-ion storage devices is still in the initial stage, and finding appropriate electrode materials is one of the most important tasks for fabricating high-performance devices. This article provides a comprehensive review on recent advances of electrode materials for emerging NH_4-ion storage devices. Firstly, the ammonium-ion batteries (AIBs) are briefly summarized, and then the cathode materials, anode materials and their NH_4-ion storage mechanism based on hydrogen bond are introduced. Furthermore, other NH_4-ion storage devices, including NH_4-ion supercapacitors (NH_4^+-SCs), NH_4-ion capacitors (AICs), ammonium dual-ion batteries (ADIBs) and ammonium-zinc hybrid batteries (AHBs), are also briefly introduced. Finally, a short conclusion and our perspectives on future developments for NH_4-ion storage device's electrodes are provided in order to promote their large-scale energy storage applications.

1. Introduction

Along with the constant consumption of fossil fuels, serious environmental pollution and the massive human demand for energy, it is urgent to search for alternative renewable and clean energy sources (*eg.* solar, wind, and tidal energy) [1,2]. Nevertheless, these green energy is intermittent and the period is highly unstable, limiting their development and wide application [3]. Therefore, large-scale development of efficient energy storage technologies is an urgent need to store the generated electricity [4]. In many energy storage technologies, batteries, especially aqueous batteries with the virtues of cost-effectiveness, environmental friendliness, high security and conductivity, have been regarded as among the most attractive devices because of their huge potential for industrial production and grid-scale applications [5–11].

At present, the charge carriers of most aqueous batteries are metal ions, including Li^+ [12], Na^+ [13], K^+ [14], Zn^{2+} [6], Mg^{2+} [15], Ca^{2+} [16], and Al^{3+} [17]. Nevertheless, the communities pay little attention to the study of non-metallic charge carriers like proton (H^+), hydronium (H_3O^+), and ammonium (NH_4^+) [18,19]. Actually, such batteries with nonmetallic ionic charge carriers can present unique properties and extraordinary performance [20]. Particularly, NH_4^+ as charge carrier yielding a mildly acidic electrolyte will avoid electrodes corrosion and suppress hydrogen evolution, which delivers much better cycling performance than H^+ and H_3O^+ [21]. In addition, compared with other metallic charge carriers, NH_4^+ displays more fascinating merits: (i) NH_4^+ is resourceful and sustainable because it can be synthesized from the infinite resources of nitrogen and hydrogen on earth [22]. (ii) it holds the lightest molar mass (18 g mol^{-1}) for high energy density batteries [21]. (iii) although it has a large ionic radius (1.48 Å), NH_4^+ possesses the smallest hydrated ionic size (3.31 Å), which is beneficial for its rapid diffusion in aqueous electrolytes [23]. (iv) ammonium salt solution is highly dissociated and therefore provides improved ionic conductivity [24]. (v) the unique interaction (hydrogen bond (H-bond)) between NH_4^+ and electrode hosts is more flexible than the rigid metal coordination [25]. (vi) the peculiar tetrahedral structure of NH_4^+ has a strong preferential orientation and thus its intercalation chemistry in host

Abbreviations: AIBs, Ammonium-ion batteries; NH_4^+-SCs, NH_4-ion supercapacitors; AICs, NH_4-ion capacitors; ADIBs, Ammonium dual-ion batteries; AHBs, Ammonium-zinc hybrid batteries; EES, Electrochemical energy storage; PBAs, Prussian blue analogues; DFT, Density functional theory; CuHCF, Copper hexacyanoferrate; PANI, Polyaniline.

* Corresponding authors.
E-mail addresses: lychen@cqu.edu.cn (L. Chen), shaowei@ucsc.edu (S. Chen).

https://doi.org/10.1016/j.cej.2023.143197
Received 20 February 2023; Received in revised form 11 April 2023; Accepted 23 April 2023
Available online 26 April 2023

materials is distinct from that of traditional spherical metal-ion carriers, thus revealing the unique electrochemical properties of ammonium-ion batteries (AIBs) [3,26].

Although the breakthrough progress has been made, AIBs still face the challenges of low energy density and limited operating potential [27]. In order to overcome these shortcomings, other ammonium-ion storage devices like NH_4-ion supercapacitors [28], NH_4-ion capacitors [29], ammonium dual-ion batteries [30], and ammonium-zinc hybrid batteries [31] have successfully attracted the interest of researchers. Electrode materials are known to be a critical factor in determining the performance of electrochemical energy storage (EES) devices. However, these emerging NH_4-ion storage devices is still in their infancy, and there are few reports on related electrode materials. Thus, the major challenge for these devices is to find appropriate electrode materials with excellent ammonium-ion storage performance to facilitate their practical application [32]. Meanwhile, the study of NH_4-ion storage mechanism of electrode materials is conducive to a deeper understanding and insight of the relationship between structure and performance [33].

Fig. 1 depicts some key advancements about electrode materials for emerging NH_4-ion storage devices. Yet up to now, there is no systematic review of recent advances in electrode materials for all emerging NH_4-ion storage devices, and what has been published is only for AIBs. For example, Passerini et al. provided a comprehensive summary on cathodes, anodes and electrolytes of AIBs [24]. On this basis, the working principle and various characterization tools of AIBs were supplemented by Jin et al. [3]. Later, although Wang et al. added some other applications of NH_4-ion storage, their electrode materials were not the focus of discussion [21]. Considering the growing attention on the electrode materials for emerging NH_4-ion storage devices in recent years, a comprehensive and in-depth review of this emerging field is very necessary.

This review focus on the recent advances of currently available cathode and anode materials for emerging NH_4-ion storage devices from mechanistic insights to practical applications. In terms of cathode materials, we focus on Prussian blue and its analogues, metal-based compounds and organic materials, while for the anode materials, we mainly introduce organic compounds, transition metal oxides and other anode compounds. A short conclusion and our perspectives on future developments for NH_4-ion storage device's electrodes are also provided.

2. Composition and working principle of AIBs

Similar with other metal-ion batteries, AIBs mainly consist of three ingredients: cathode, anode and electrolytes. In addition, a separator is arranged between the cathode and anode, avoiding short circuit caused by direct contact of the two electrodes. In general, cathode materials mainly include Prussian blue analogues (PBAs) with high working voltage, V-based oxides with long-term cycle life, and Mn-based materials with remarkable rate capability as well as organic materials with rich variety. Of course, organic materials, transition metal oxides/sulfides and so on are also suitable for anode materials. Besides, electrolytes frequently used in aqueous AIBs include $(NH_4)_2SO_4$, NH_4NO_3, NH_4Cl, and NH_4Ac. According to their solubility, different concentrations of electrolytes were obtained and used in various electrode system [34].

Fig. 2 shows the working principle of AIBs. Generally speaking, it is presented that NH_4-ions commute back and forth between the cathode and anode inside the batteries. Specifically, during charging process, NH_4^+ ions are released from the cathode and move across the separator and electrolyte to anode, while electrons with the same amount of charge in the cathode also migrate to anode through the external circuit. Ultimately, the ammonium-ions and electrons that reach the anode react with the anode and charging is finished. Thus, charging is the process of converting electrical energy into chemical energy, which is stored in the battery by means of chemical bonds. While the discharge behavior is exactly the opposite, *i.e.* ammonium-ions and electrons are released from the anode back to cathode and both combined with the cathode, and discharging process is complete. At this point, chemical energy previously stored in the battery is released in the form of electrical energy to power the external electronic devices. According to such a reversible operation mechanism, the electrochemical performance of AIBs is largely determined by the properties of electrode materials [3]. Therefore, the study of the practical applications and mechanistic insights of electrode materials is crucial and researchers have put great efforts on it.

3. Cathode materials for AIBs

As we all know, cathode materials are more critical in terms of the capacity of batteries than anode materials. Therefore, it is of great significance to develop high-performance cathode materials for emerging

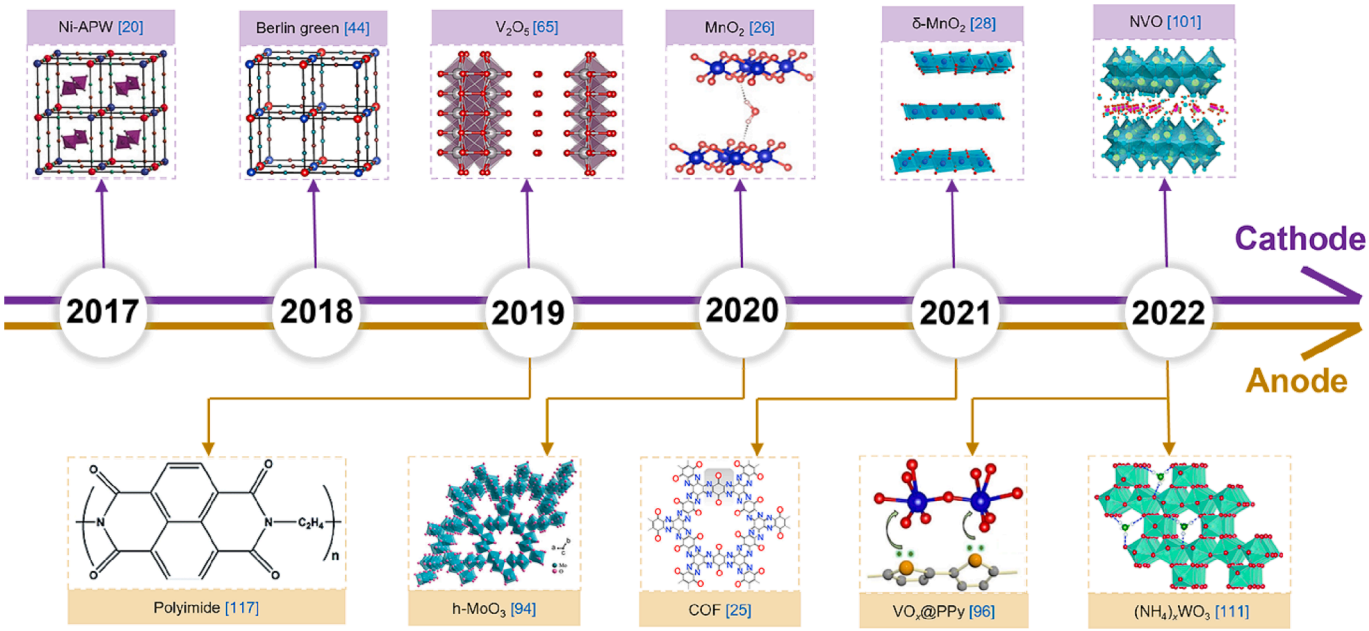

Fig. 1. Timeline of the representative cathode and anode materials for emerging NH_4-ion storage devices.

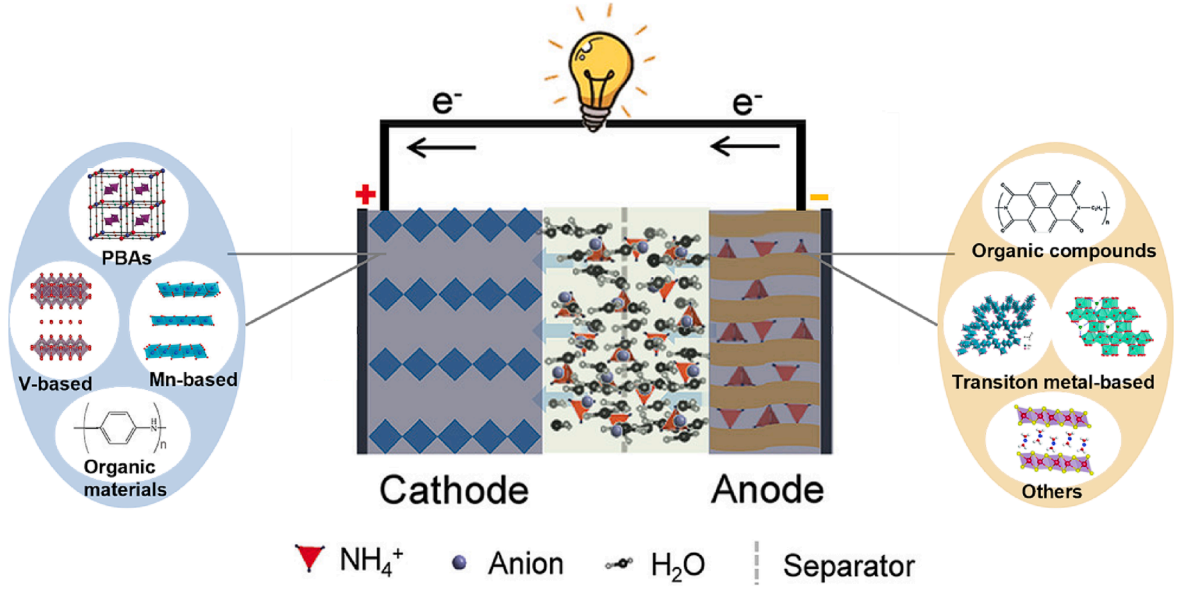

Fig. 2. Schematic diagram of ammonium ion battery.

AIBs to improve their capacity. Researchers have made great efforts and contributions in this respect. Up to now, besides PBAs, metal-based compounds and organic materials are regarded as the most promising materials. Table 1 has listed the various cathode materials and the corresponding performance for aqueous AIBs.

3.1. Prussian blue and its analogues

Because K^+ and NH_4^+ have almost the same hydrated size and ionic radius, the cathode selection of AIBs is to some extent similar to that of K-ion batteries. As the first prototype of K-ion batteries, the choice of PBAs as the cathode first attracted the attention of researchers [35,36]. The chemical formula of PBAs is $A_xM'_y[M(CN)_6]_{1-y}{\cdot}nH_2O$, where A = alkali metal, M/M' = transition metals, $0 \le x \le 2$, $y < 1$. In particular, when M = M' = Fe, the end product is Prussian blue (PB). M and M' are bonded by CN ligands respectively to form a 3D open-framework structure [37]. PBAs with this unique structure can deliver impressive rate capability and ultra-long cycling [38], which makes them the good candidates for NH_4^+ ion storage. This part will introduce the performance of PB and some representative PBAs as cathode materials for AIBs and their NH_4-ion storage mechanism.

3.1.1. Prussian blue and its NH_4-ion storage mechanism

In 2020, Shu et al. synthesized PB ($Fe_4[Fe(CN)_6]_3$) through co-precipitation route and focused on evaluating the role of NH_4^+ intercalation on its stability in aqueous AIBs based on density functional theory (DFT) calculations [39]. It was found that the H-bonds formed between NH_4^+ and N of $Fe_4[Fe(CN)_6]_3$ played an key role in the stability of the system (Fig. 3a). It is well known that the storage principles of PB in batteries are mainly based on transition metal redox and intercalation mechanism [40]. Shu's group revealed that the corresponding NH_4-ion storage mechanism is associated with the reduction of two Fe^{3+} ions to Fe^{2+} ions per formula unit, together with the intercalation of two NH_4^+ ions into the lattice of PB, based on the reaction equation given by [39]:

$$Fe_4^{3+}[Fe^{2+}(CN)_6]_3 + 2e^- + 2NH_4^+ \leftrightarrow (NH_4)_2Fe_2^{2+}Fe_2^{3+}[Fe^{2+}(CN)_6]_3 \quad (1)$$

To go further, the *in-situ* XRD patterns (Fig. 3b and c) were collected in a complete cycle under different charge/discharge states to demonstrate that PB has a highly reversible structural evolution during NH_4^+ intercalation, which involved a solid-solution reaction mechanism [39]. Taking advantage of the merits mentioned above, $Fe_4[Fe(CN)_6]_3$ exhibited distinguished capacity of 46.7 mAh g^{-1} at 20 C.

In another study, Li et al. controlled synthesis of ball-cutting $NaFe^{III}[Fe^{II}(CN)_6]$ (Na-FeHCFs) nanocubes by changing the stirring speed of the solution (Fig. 3d) [41]. Electrochemical tests demonstrated their unmatched cycling stability and excellent cycling performance (Fig. 3e). From the cyclic voltammetry (CV) results (Fig. 3f), it can be speculated that the superior performance of Na-FeHCFs can be attributed to the reversible redox reaction of the high-spin nitrogen-coordinated Fe^{II}/Fe^{III} (Fe^{H}) pair. The reaction mechanism involved in Na-FeHCFs can be described as follows [41]:

$$NaFe^{III}[Fe^{II}(CN)_6] + NH_4^+ + e^- \leftrightarrow Na(NH_4)Fe^{II}[Fe^{II}(CN)_6] \quad (2)$$

Typically, PB can be directly transformed between Prussian green (PG, $Fe^{III}[Fe^{III}(CN)_6]$) and Prussian white (PW, $K_2Fe^{II}[Fe^{II}(CN)_6]$) by electrochemical redox reactions [42,43]. In 2018, Berlin green (BG, $Fe[Fe(CN)_6]$) framework showed better structural compatibility for hosting NH_4^+ ions compared to Na^+ ions and K^+ ions (Fig. 3g) according to the study of Ji et al. [44], which is reflected by higher operation potential and the structural feature of NH_4^+ insertion with almost zero strain. Therefore, the BG electrode displayed remarkable long-term cycle life with 78% capacity retention after 50 000 cycles. Besides, Shu's group added $Fe_2(SO_4)_3$ into $NH_4(SO_4)_2$ electrolyte, which made $FeFe(CN)_6$ cathode with a rate retention of 96.3% after nearly 1000 cycles (Fig. 3h), confirming the importance of the "common ion effect" [45] formed by the appropriate amounts of electrolyte additives for the improvement of electrochemical performance [46]. Similar to PB, all XRD spectra of PG showed a consistent face-centered cubic structure, manifesting also the existence of solid solution reaction during NH_4^+ intercalation [46]. The electrochemical reaction mechanism of reversible phase transition between $Fe^{III}[Fe^{III}(CN)_6]$ and $(NH_4)Fe^{II}[Fe^{III}(CN)_6]$ during charge–discharge processes was disclosed as follows [44,46]:

$$Fe^{III}[Fe^{III}(CN)_6] + NH_4^+ + e^- \leftrightarrow (NH_4)Fe^{II}[Fe^{III}(CN)_6] \quad (3)$$

3.1.2. PBAs and their NH_4-ion storage mechanism

PBAs are derived from the ligand PB with strong open frameworks. Specifically, PBAs can be synthesized by using transition metals (Ni, Cu, Mn, V, *etc.*) to substitute Fe in PB [47]. Several common PBAs for NH_4^+ ion storage, such as nickel hexacyanoferrate, copper hexacyanoferrate, manganese hexacyanoferrate, *etc.*, will be introduced in the following.

Table 1
Summary of various cathode materials and the corresponding performance for AIBs.

Materials	Electrolyte	Voltage range	Specific capacity (current density)	Cycling stability (cycles, current density)	Ref.
$Fe_4[Fe(CN)_6]_3$	1M $(NH_4)_2SO_4$	0.1–1.0 V vs. Ag/AgCl	40 mAh·g^{-1} (1.8 A·g^{-1})	88.9% (2000, 1.8 A g^{-1})	[39]
Na-FeHCFs	1M $(NH_4)_2SO_4$	0–0.7 V vs. SCE	62 mAh g^{-1} (0.25 A g^{-1})	109.7% (50 000, 2 A g^{-1})	[41]
Berlin Green	0.5M $(NH_4)_2SO_4$	−0.2–1.2 V vs. Ag/AgCl	80 mAh g^{-1} (5 A g^{-1})	78% (50 000, 5 A g^{-1})	[44]
$FeFe(CN)_6$	0.1M $Fe_2(SO_4)_3$ + $(NH_4)_2SO_4$	0.2–0.8 V vs. Ag/AgCl	72 mAh g^{-1} (0.8 A g^{-1})	96.3% (1000, 0.2 A g^{-1})	[46]
NiHCF	0.5M $(NH_4)_2SO_4$	0.4–1.0 V vs. SHE	38 mAh g^{-1} (0.5 A g^{-1})	88% (500, 0.5 A g^{-1})	[49]
CuHCF	0.5M $(NH_4)_2SO_4$	0.6–1.4 V vs. SHE	55 mAh g^{-1} (0.5 A g^{-1})	91% (500, 0.5 A g^{-1})	[49]
Ni-APW	1M $(NH_4)_2SO_4$	0.2–0.9 V vs. Ag/AgCl	51.3 mAh g^{-1} (0.3 A g^{-1})	74% (2000, 0.3 A g^{-1})	[20]
$Ni_2Fe(CN)_6$	2M NH_4Cl	0.1–0.9 V vs. Ag/AgCl	60.3 mAh g^{-1} (1C)	—	[50]
$Na_{1.5}Ni_{1.25}Fe(CN)_6$	1M NH_4NO_3	0–1.0 V vs. Ag/AgCl	56.1 mAh g^{-1} (1C)	93.2% (150, 1C)	[51]
$Ni_2Fe(CN)_6$	1M NH_4NO_3	0–1.0 V vs. Ag/AgCl	57.3 mAh g^{-1} (1C)	78.2% (1000, 10C)	[52]
NiHCF@CNTs	19M CH_3COONH_4	0–0.9 V vs. Ag/AgCl	44 mAh g^{-1} (1 A g^{-1})	90% (300, 2 A g^{-1})	[54]
PNFF-60	1M $(NH_4)_2SO_4$ + 1 mM $NiSO_4$	−0.2–1.0 V vs. Ag/AgCl	92.5 mAh g^{-1} (0.1 A g^{-1})	95.2% (1000, 2 A g^{-1})	[55]
N-CuHCF	2M NH_4NO_3 + 0.01M $Cu(NO_3)_2$	0.5–1.0 V vs. SCE	53.1 mAh g^{-1} (10 A g^{-1})	91.5% (17 000, 10 A g^{-1})	[56]
CuHCF	2M NH_4NO_3	0.3–1.1 V vs. SCE	74.9 mAh g^{-1} (0.1 A g^{-1})	72.5% (30 000, 5 A g^{-1})	[57]
N-CuHCF	5.8 m $(NH_4)_2SO_4$	0.4–1.0 V vs. Ag/AgCl	42.4 mAh g^{-1} (1.2 A g^{-1})	85% (800, 0.6 A g^{-1})	[58]
K-V-Fe PBAs	1M $(NH_4)_2SO_4$	−0.1–1.2 V vs. SCE	92.85 mAh g^{-1} (2 A g^{-1})	91.44% (2000, 2 A g^{-1})	[60]
MnHCF	1M NH_4TFSI/TEGDME	0–1.0 V vs. Ag/Ag^+	104 mAh g^{-1} (0.1 A g^{-1})	98% (100, 0.1 A g^{-1})	[61]
FeMnHCF	24 m $NH_4CF_3SO_3$	−1.0–1.8 V vs. Ag/AgCl	123.8 mAh g^{-1} (0.5 A g^{-1})	68.5% (10 000, 3 A g^{-1})	[62]
V_2O_5	0.5M $(NH_4)_2SO_4$	−0.2–0.8 V vs. Ag/AgCl	70 mAh g^{-1} (5 A g^{-1})	80% (30 000, 5 A g^{-1})	[65]
PVO	0.5M $(NH_4)_2SO_4$	−0.5–0.9 V vs. SCE	307 mAh g^{-1} (0.5 A g^{-1})	42% (100, 5 A g^{-1})	[68]
PVO	0.5M $(NH_4)_2SO_4$	−0.5–1.0 V vs. Ag/AgCl	192.5 mAh g^{-1} (1 A g^{-1})	98% (100, 10 A g^{-1})	[22]
Co-doped V_2O_5	0.5M $(NH_4)_2SO_4$	−1.8–1.8 V vs. Ag/AgCl	172 mAh g^{-1} (1 A g^{-1})	61.6% (500, 1 A g^{-1})	[69]
$CF@NH_4V_4O_{10}$	1M $(NH_4)_2SO_4$	0.01–1.0 V vs. Ag/AgCl	103 mAh g^{-1} (0.1 A g^{-1})	82.5% (100, 0.1 A g^{-1})	[71]
$NH_4V_3O_8{\cdot}2{\cdot}.9H_2O$	1M $(NH_4)_2SO_4$	0–1.0 V vs. Ag/AgCl	110 mAh g^{-1} (0.1 A g^{-1})	95% (400, 0.1 A g^{-1})	[72]
FVO	0.5M $(NH_4)_2SO_4$	−0.4–1.2 V vs. SHE	72.5 mAh g^{-1} (5 A g^{-1})	61% (500, 5 A g^{-1})	[73]
Hetero-VS_2/VO_x	5M $(NH_4)_2SO_4$	−0.6–0.9 V vs. Ag/AgCl	200 mAh g^{-1} (0.1 A g^{-1})	43% (1000, 1 A g^{-1})	[27]
MnO_x	0.5M NH_4Ac	0–0.8 V vs. SCE	176 mAh g^{-1} (0.5 A g^{-1})	94.7% (10 000, 5 A g^{-1})	[26]
MP-20	1M NH_4Ac	−0.1–0.9 V vs. SCE	299.6 mAh g^{-1} (1 A g^{-1})	96.3% (500, 2 A g^{-1})	[78]
ES-PANI/CFs	0.5M $(NH_4)_2SO_4$	−0.2–0.8 V vs. Ag/AgCl	160 mAh g^{-1} (1 A g^{-1})	82% (100, 5 A g^{-1})	[79]

Note: Ni-APW, $(NH_4)_{1.47}Ni[Fe(CN)_6]_{0.88}$; PNFF-60, PANI/$Na_{0.73}Ni[Fe(CN)_6]_{0.88}$ with 60 μL of aniline; NH_4TFSI/TEGDME, bis(trifluoromethane)sulfonimide ammonium/tetraethylene glycol dimethyl ether; PVO, polyaniline (PANI) intercalated V_2O_5; CF, carbon fiber; FVO, ferric vanadate oxide; MP-20, $(NH_4)_{0.27}MnO_{1.04}(PO_4)_{0.28}$; ES-PANI/CFs, emeraldine salt polyaniline on carbon felts; SCE, saturated calomel electrode; SHE, saturated hydrogen electrode.

3.1.2.1. Nickel hexacyanoferrate (NiHCF). NiHCF with large channel structure is one of the potential PBAs cathode material for aqueous batteries [48]. In Cui's work, the NH_4^+ storage performance of NiHCF was first investigated [49]. By comparing the CV and galvanostatic cycling electrochemical response behavior (Fig. 3i), they found that the intercalation potential of NH_4^+ is highest among NH_4^+, Li^+, Na^+ and K^+. Subsequently, Ji et al. also proposed the $(NH_4)_{1.47}Ni[Fe(CN)_6]_{0.88}$ (Ni-APW) as cathode material, which presented good long-term cycling performance and high capacity retention of 74% within 2000 cycles at 5C (Fig. 3j) [20]. More importantly, they created the first "rocking-chair" NH_4-ion full battery by using the Ni-APW cathode and the PTCDI anode, which exhibited an operation voltage of 1 V (Fig. 3k) and an energy density of 43 Wh kg^{-1}.

In 2021, Yu and coworkers successfully prepared $Ni_2Fe(CN)_6$ via co-precipitation method and studyed the topochemistry of NH_4^+ during the electrochemical reaction, from which they found that its initial Coulombic efficiency was as high as 122.9% [50]. To overcome this problem, Yu et al. proposed to reduce a small amount of $Fe(CN)_6^{3-}$ in $Ni_2Fe(CN)_6$ electrode with ascorbic acid, which reduced the initial Coulombic efficiency to 95.9%, accompanied by the improvement of electrochemical performance. In 2022, their group optimized the structure of $Ni_2Fe(CN)_6$ by partially replacing nickel with sodium, and its electrochemical properties of a range of $Na_{2x}Ni_{2-x}Fe(CN)_6$ (x = 0, 0.25, 0.5, 0.75, and 1) materials was investigated [51]. Surprisingly, $Na_{0.5}Ni_{1.75}Fe(CN)_6$ has the highest diffusion coefficient among all samples, while $Na_{1.5}Ni_{1.25}Fe(CN)_6$ shows the longest cycling life with 93.2% capacity retention after 150 cycles. The results showed that partial Na doping optimized the electrochemical performance of $Na_{2x}Ni_{2-x}Fe(CN)_6$. This pre-insertion proved to be an effective strategy in battery systems to enhance structural stability and ionic conductivity, thereby accelerating NH_4^+ diffusion and providing stable cycling performance. In addition to the design of electrode structure, their group also explored the effect of different anions in electrolytes [NH_4NO_3,

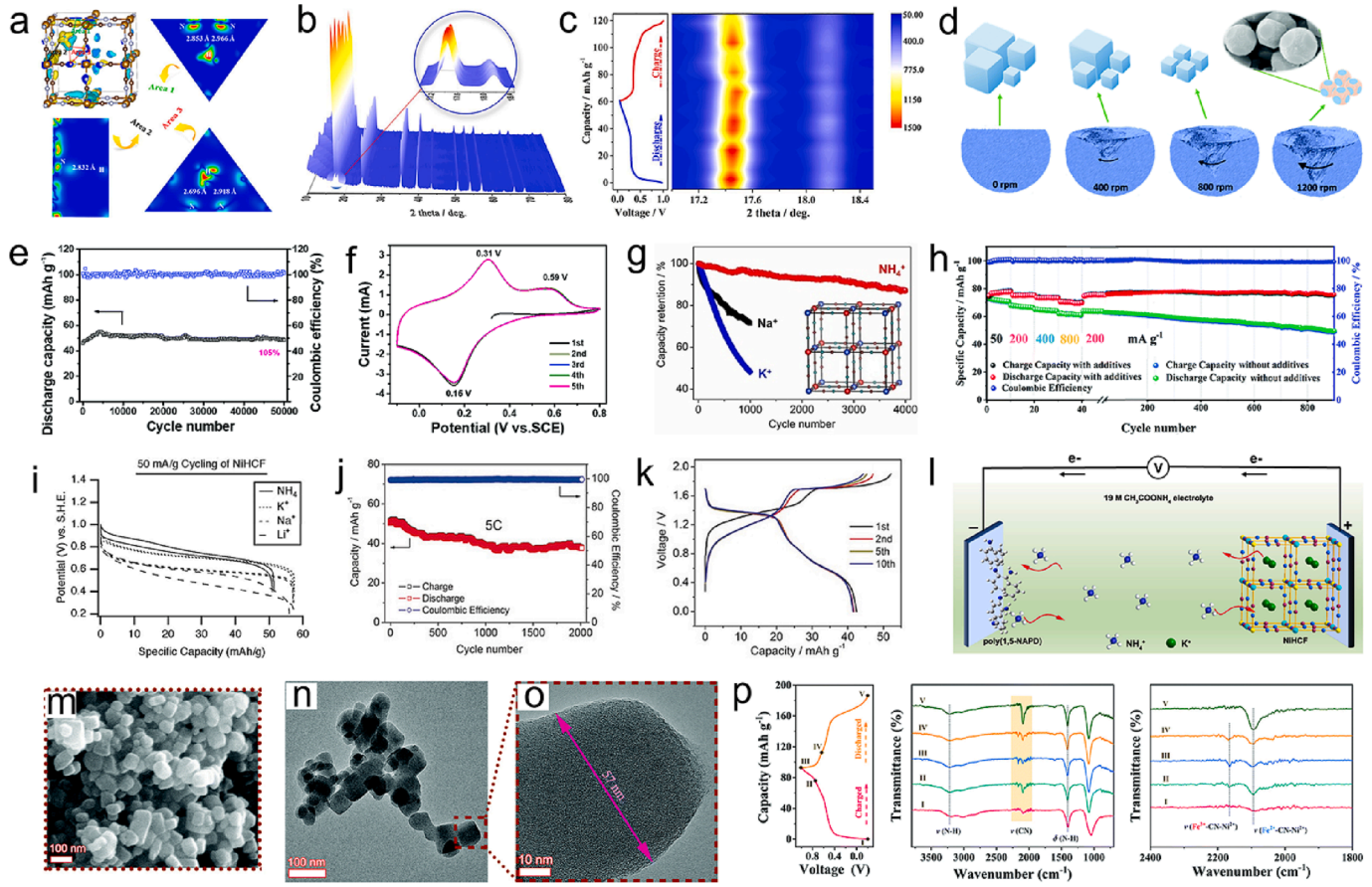

Fig. 3. (a) The 3D electron density difference (ρ-$\rho_{corr.}$) and its 2D slices across Area 1, Area 2, and Area 3. (b) Overall XRD spectra at different charge/discharge states in a full cycle and the inset is the enlarged view of 17.0–18.5°. (c) Typical GCD curves and corresponding XRD color map in 17.0–18.5° (a-c) Reproduced with permission [39]. Copyright 2020, Elsevier. (d) Schematic illustration of the synthesis of Na-FeHCFs with tailored morphology by changing the stirring speed. (e) Long-term cycling performance at 2 A g^{-1} and (f) the first five CV curves at 5 mV s^{-1} of a ball-cutting Na-FeHCF electrode. (d-f) Reproduced with permission [41]. Copyright 2019, The Royal Society of Chemistry. (g) Capacity retention of Berlin green for Na^+, K^+, and NH_4^+ storage at 1 A g^{-1}. Reproduced with permission [44]. Copyright 2018, American Chemical Society. (h) Rate performance with and without the $Fe_2(SO_4)_3$ additive of FeHCF. Reproduced with permission [46]. Copyright 2021, The Royal Society of Chemistry. (i) The potential profiles of NiHCF during galvanostatic cycling of Li^+, Na^+, K^+, and NH_4^+, at 50 mA g^{-1}. Reproduced with permission [49]. Copyright 2011, The Electrochemical Society. (j) Long-term cycling performance at 5C of Ni-APW cathode. (k) Selected GCD profiles from the initial 10 cycles at a current density of 60 mA g^{-1} of aqueous NH_4-ion battery. Reproduced with permission [20]. Copyright 2017, Wiley-VCH. (l) Schematic illustration of the reaction mechanism of the NiHCF@CNTs//poly(1,5-NAPD) full cell. Reproduced with permission [54]. Copyright 2021, Elsevier. (m) SEM image; (n) and (o) TEM images; (p) Typical GCD profiles and corresponding ex situ FTIR analysis of the PNFF-60 cathode. (m-p) Reproduced with permission [55]. Copyright 2022, The Royal Society of Chemistry. (For interpretation of the references to color in this figure legend, the reader is referred to the web version of this article.)

NH_4Cl, and $(NH_4)_2SO_4$] on the electrochemical performance of $Ni_2Fe(CN)_6$ for aqueous AIBs [52]. The results indicate that under the same NH_4^+ concentration, $Ni_2Fe(CN)_6$ exhibits better performance in 1 M NH_4NO_3 than in 0.5 M $(NH_4)_2SO_4$ and 1 M NH_4Cl, which is due to the rhombohedral phase of $Ni_2Fe(CN)_6$ in $(NH_4)_2SO_4$ electrolyte and the strong coordination ability of chloride, respectively. We can clearly see that in the electrolyte with the same cationic concentration, different anions have different effects on the properties of the host materials. Based on this, we can adjust the type of electrolyte to achieve the best performance of the electrode materials.

To overcome the limitation caused by the inherent defects of PBAs, researchers have tried to combine them with functional materials to enhance the electrochemical performance [37,53]. For instance, Wang et al. applied NiHCF@CNTs cathode and poly(1,5-naphthalenediamine) anode to assemble the aqueous AIB, in which NH_4^+ acted as a charge carrier, performing an encouraging energy density of 31.8 Wh kg^{-1} and showing a rocking-chair mechanism [54]. As shown in Fig. 3l, during the first charge, K^+ ions were extracted from the NiHCF@CNTs cathode, and NH_4^+ ions were inserted into the poly(1,5-NAPD) anode via a coordination reaction. Subsequently, it was mainly NH_4^+ ions that continued to shuttle in the electrolyte, cathode and anode [54]. In addition, Yang et al. obtained PANI/$Na_{0.73}Ni[Fe(CN)_6]_{0.88}$ with 60 μL of aniline (PNFF-60) with regular cubes and edge lengths of about 57 nm (Fig. 3m-o) by interface and electronic structure engineering [55]. Benefiting from inheriting the virtues of high conductivity of PANI and stability of PBAs, the PNFF-60 can reach 95.2% capacity retention after 1000 cycles even at 2000 mA g^{-1} when used as a cathode for AAIBs. The NH_4^+ storage mechanism of PNFF-60 was also analyzed. From the FT-IR spectrum (Fig. 3p), upon charging, a new peak at 2164 cm^{-1} can be found, which is due to the vibration of Fe^{3+}–CN–Ni^{2+}. This new peak disappeared during discharge, revealing a reversible redox reaction mechanism [55].

Although the progress of NiHCF as a cathode material for AIBs has been generally recognized, the internal defects of NiHCF are still a long-term problem for researchers to overcome. In addition to the solution of composite preparation, defect engineering and doping engineering can also be regarded as the powerful means to improve the performance of host materials, which is worthy of further exploration.

3.1.2.2. Copper hexacyanoferrate (CuHCF). CuHCF is a class of materials with a Prussian blue-like crystal structure, extensively used for energy storage [40,47], and now it is also gradually emerging in the field of ammonium ion energy storage. In early 2012, Cui et al. demonstrated

that CuHCF has a higher intercalation potential of NH_4^+ (1.02 V vs. S.H.E.) than that of Li^+, Na^+ and K^+ [49]. Their results imply that aqueous AIBs are ideal electrochemical energy storage devices.

Time comes, Shu's team prepared NH_4^+-rich CuHCF (N-CuHCF), but its capacity value was relatively low [56]. Fortunately, $Cu(NO_3)_2$ electrolyte additive overcame this problem and endowed N-CuHCF with excellent capacity retention of 91.5% over 17 000 cycles at 100 C (Fig. 4a). Besides, the storage mechanism of quasi-solid-solution reaction on the basis of Fe^{3+}/Fe^{2+} and Cu^{2+}/Cu^+ pairs was uncovered by various characterization methods [56]. To go further, the NH_4^+ storage and diffusion mechanism in CuHCF was disclosed by their team, who applied the advanced characterization technique such as *in-situ* XRD and *ex situ* XPS to describe the reversible redox reaction mechanism formulated as follows [57]:

$$Cu_{2.95}[Fe^{III}_{0.75}Fe^{II}_{0.25}(CN)_6]_{1.69}+2e^-+2NH_4^+\leftrightarrow(NH_4)_2Cu_{2.95}[Fe^{II}(CN)_6]_{1.69} \quad (4)$$

Meanwhile, the building and breaking of H-bonds during the ammoniation/de-ammoniation progresses is an intrinsic property of fast charge transfer, which has been confirmed by *ex-situ* FTIR, SSNMR and theoretical calculation [57]. Furtherly, the activation energy of each diffusion step was calculated (Fig. 4b), and the diffusion process of NH_4^+ was expounded (Fig. 4c). Once NH_4^+ is inserted into the 48 g site of CuHCF, a H-bond is formed between the H of NH_4^+ and the N in CuHCF. As NH_4^+ diffuses between two adjacent 48 g sites, a new H-bond will be formed [57]. Similarly, Passerini et al. designed a stable AAIB based on N-CuHCF cathode, PTCDI anode, and 5.8 m $(NH_4)_2SO_4$ electrolyte to improve cycling performance, which provided ca. 72% capacity retention over 1000 cycles and an output potential of about 1 V [58].

According to the current reports on CuHCF, although it was used earlier as the electrode materials for ammonium ion energy storage, it is a pity that it did not get more attention in the later period. In fact, CuHCF itself more excellent properties is worth researchers to continue to develop, in order to meet the needs of industrial production and application.

3.1.2.3. Others. Apart from NiHCF and CuHCF materials, other PBAs have also been used in AAIBs in recent years. For instance, V-PBAs have been developed as electrode materials by researchers [59]. In 2021, Xing and coworkers synthesized novel K-V-Fe PBAs nanocubes to ensure improved structural stability and electrochemical activity of PBAs [60]. The materials could perform a encouraging specific capacity (92.85 mAh g^{-1}) and a long cycle life (Fig. 4d), indicating promising application prospect of doping strategy in PBAs. Next year, Zhang's group was the first to report the novel organic NH_4^+ ion batteries, verifying the feasibility of using NH_4^+ ions as charge carriers in organic electrolytes [61]. Notably, MnHCF as cathode displayed excellent electrochemical performance, delivering a reversible capacity of 104 mAh g^{-1} at 100 mA g^{-1} with 98 % retention over 100 cycles (Fig. 4e) and good rate performance. In addition, its NH_4^+ ion storage mechanism related to the $Fe^{2+/3+}$ and $Mn^{2+/3+}$ redox reactions was systematically illustrated by combining *ex-situ* XRD and XPS [61]. In FeMnHCF, Mn^{3+}/Mn^{2+}-N redox reaction at high potential was introduced, which not only endows the cathodes with high voltage but also provides more capacity [62].

Although this kind of material has shown excellent electrochemical behaviors, its specific capacity is still limited and uncompetitive. Fortunately, the specific capacity of PBAs electrode can be improved by introducing the multivalent metals (for example V, Mn, Co, *etc.*) at the M' site to design the multi-pair redox. Therefore, PBAs electrode like VHCF, MnHCF and CoHCF should be more developed in the future research.

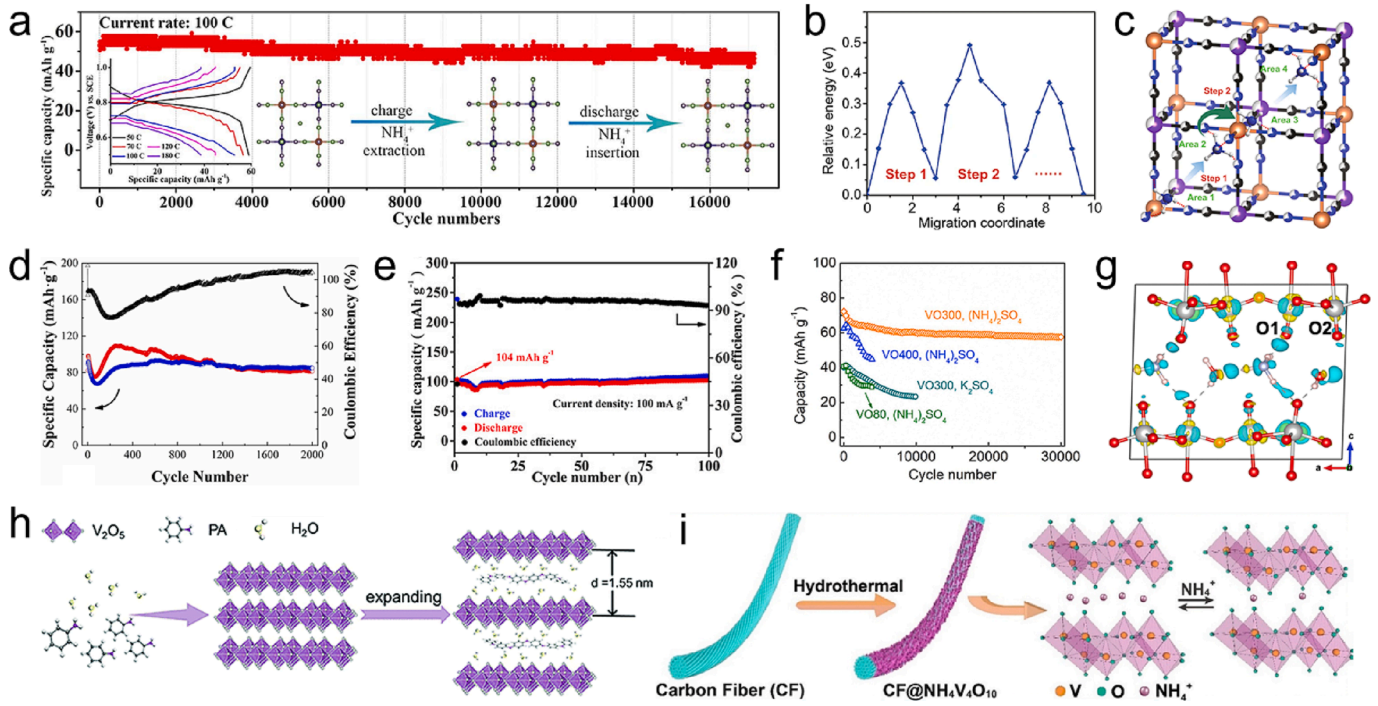

Fig. 4. (a) Long-term cycling performance of N-CuHCF electrodes at C-rate of 100C. Reproduced with permission [56]. Copyright 2021, Elsevier. (b) Changes of diffusion activation energy during ammoniation/deammoniation progresses. (c) Schematic illustration of NH_4^+ diffusion from 48 g site to another. (b, c) Reproduced with permission [57]. Copyright 2021, Springer Nature. (d) Cycling test results at 2 A·g^{-1} of K-V-Fe PBAs NCs/CC electrode. Reproduced with permission [60]. Copyright 2020, Elsevier. (e) Cycling performance at 100 mA g^{-1} of MnHCF. Reproduced with permission [61]. Copyright 2022, Wiley-VCH. (f) Long-term cycle life of V_2O_5 electrodes in $(NH_4)_2SO_4$ and K_2SO_4 electrolytes at 5 A g^{-1}. (g) Plots of charge density difference for the ammoniated V_2O_5 electrode, showing the movement of charge derived from the host–guest interaction. (f, g) Reproduced with permission [65]. Copyright 2019, Elsevier. (h) Illustration of the synthesis process for PVO. Reproduced with permission [68]. Copyright 2022, The Royal Society of Chemistry. (i) Schematic illustration of the CF@ urchin-like $NH_4V_4O_{10}$ and the evolution of the structure. Reproduced with permission [71]. Copyright 2019, Elsevier.

3.2. Metal-based compounds and their NH_4-ion storage mechanism

Aside from PB and PBAs, metal-based compounds (*eg.* V-based oxides, Mn-based compounds) also have been commonly used as another type of cathode materials for AIBs. On one hand, most of them with wide interlayer structure or large open structure can provide sufficient ion channels for great storage capacity. On the other hand, transition metals with various valence states can form stable structures with other ions [21]. The above two points can achieve high storage capacity. More importantly, the storage mechanism of forming/breaking of strong hydrogen bonds between metal-based compounds and NH_4^+ also contributes to the rapid NH_4^+ storage capability.

3.2.1. V-based oxides

V-based oxides show great promise for aqueous AIBs because the various valences of V element ($V^{5+} \leftrightarrow V^{4+} \leftrightarrow V^{3+}$) can realize multi-electron transfer during redox process and obtain high capacity, which can compensate for the low capacity of PBAs [63,64]. Ji's group. obtained three different V_2O_5 structures VO80, VO400, and VO300, in which the VO300 electrode can achieve longer cycling life (only 20% NH_4^+ capacity loss after 30 000 GCD cycles at 50 C) compared to the VO80 and VO400 electrodes (Fig. 4f) although all V_2O_5 electrodes have similar reversible capacities of ≈ 100 mAh g^{-1} at 1 C [65]. In depth, DFT calculations offered further mechanism insights for a non-diffusion-controlled pseudocapacitive behavior of ammonium migrating in V_2O_5 structure. From the Fig. 4g, we can see that a small amount of charge in the reduced V_2O_5 electrode is transferred from V to H···O=V bond through the bonded O=V bond, resulting in V oxidation [65]. During charge–discharge process, the total energy required to form $(NH_4)_{0.5}V_2O_5{\cdot}0.5H_2O$ (−287.464 eV) is lower than that needed to form $K_{0.5}V_2O_5{\cdot}0.5H_2O$ (−246.245 eV) due to different energy storage mechanisms [65]. It is precisely because of the easy formation and fracture of H-bonds between NH_4^+ and V_2O_5 layers that V_2O_5 has a faster storage capacity for NH_4^+ than other metallic charge carriers (such as K^+). In addition, they also discovered that the effect of the interlayer spacing of V_2O_5 on its NH_4^+ storage cannot be ignored. Studies have shown that vanadium oxide with larger interlayer spacing is beneficial to expose more active sites and offer wider ion channels, and exhibit greater storage capacity [66,67]. With this context, Mai et al. prepared polyaniline (PANI) intercalated V_2O_5 (PVO) with an expanded layer of 1.55 nm by one-step hydrothermal route (Fig. 4h) for NH_4-ion batteries, showing the highest ever reported capacity of ca. 307 mAh g^{-1} at 0.5 mA g^{-1} [68]. Similarly, Wang's group prepared the PVO with an interlayer spacing of 13.99 Å between V-O layers [22]. Moreover, a high capacity (192.5 mAh g^{-1} at 1 A g^{-1}) and superior cycling stability were obtained by optimizing PVO electrode. Besides, Xiang's team also discovered that Co-doped V_2O_5 cathode can potentially help to increase the electronic conductivity of AIBs, indicating that metal atom doping is a feasible way for rapid electron transfer [69].

To rapidly promote the practical application of AIBs, the researchers focused on finding layered ammonium vanadate materials that can accommodate and reversibly release large amounts of NH_4^+ ions [70]. For instance, Li's group employed urchin-like $NH_4V_4O_{10}$ (Fig. 4i) as cathode and PANI as anode in $(NH_4)_2SO_4$ electrolyte to assemble a full AIB [71]. The aqueous AIB could show a high specific capacity of 167 mAh g^{-1} at 0.1 A g^{-1}. However, aqueous electrolyte may produce side reactions caused by water hydrolysis, thus affecting the lifespan of batteries [72]. To solve this problem, Wang et al. assembled a full flexible AIB arranging a concentrated hydrogel electrolyte sandwiched between the $NH_4V_3O_8{\cdot}2{\cdot}9H_2O$ nanobelts cathode and the PANI anode [72]. Results show that the battery with the gel electrolyte displays a capacity of 60 mAh g^{-1} with 88% capacity retention after 250 cycles at 0.1 A g^{-1} [72].

In addition, Xu's group first introduced layered iron vanadate (FVO) nanosheets as NH_4^+ ion storage electrode, manifesting a specific capacity of 72.5 mAh g^{-1} at 5 A g^{-1} [73]. In addition, NH_4^+ insertion also involved the formation of H-bonds between NH_4^+ ions and FVO nanosheets [73]. To enhance charge separation efficiency and boost electronic transportation, Du's team in situ constructed a heterostructural VS_2/VO_x cathode material (Fig. 5a-d) [27]. Thanks to the internal electric field at heterogeneous interfaces, the heterostructural VS_2/VO_x provided higher capacity above 150 mA g^{-1} at 0.1 A g^{-1} compared to VS_2 (Fig. 5e).

3.2.2. Mn-based compounds

Except for V-based oxides, Mn-based compounds are also worthy of attention. It is well known that Mn-based compounds are mature materials for aqueous batteries [74,75], especially for Zn-ion batteries [76]. Liu and his colleagues were the first to introduce an electrodeposited manganese oxide (MnO_x) cathode for NH_4^+ storage [26]. A solid-solution behavior of the reversible NH_4^+ insertion/deinsertion associated with continuous formation/destruction of H-bonds between NH_4^+ ions and the layered MnO_x was described by systematically experimental and theoretical studies (Fig. 5f-g). As displayed in Fig. 5h, the outstanding performance of the MnO_x with a high capacity of 66 mAh g^{-1} even at 10 A g^{-1} was observed in 0.5 M NH_4Ac electrolyte [26]. Given its fast ion diffusion and high output potential, manganese phosphate is another promising Mn-based compound as cathode material for aqueous batteries such as aqueous Na-ion batteries [77]. Liu's group also created a porous amorphous manganese phosphate material (MP-20) by electrochemical treatment (Fig. 5i) for NH_4^+ storage [78]. Meanwhile, a novel NH_4^+/H^+ co-intercalation mechanism of MP-20 electrode in 1 M NH_4Ac electrolyte was given. It is the coordination effect of Ac^- in NH_4Ac electrolyte that can greatly tune the surface properties of electrodes and improve electrochemical performance [78]. As a result, the MP-20 electrode exhibited an unprecedentedly high specific capacity of 299.6 mAh g^{-1} at 1 A g^{-1}.

3.3. Organic materials and their NH_4-ion storage mechanism

Organic materials have been developed as cathode materials for various aqueous batteries because of their molecular-level controllability and structural diversity, as they can store cations in conjugated chemical bonds during discharge [79–81]. Among them, polyaniline (PANI) has aroused great attention owing to its high electrical conductivity, high Coulombic efficiency, benign environment, low cost, and easy synthesis [81,82]. For instance, Wang et al. utilized *in-situ* polymerization to synthesize emeraldine salt polyaniline on carbon felts (ES-PANI/CFs) as cathode for NH_4^+ storage [79]. Fig. 5j and k illustrated the intercalation process of NH_4^+ in the electrode ES-PANI doped with Cl^- ions using 0.5 M $(NH_4)_2SO_4$ electrolyte. During charge–discharge, the interaction between NH_4^+ and $-SO_3^-$ or $-SO_4^{2-}$ was confirmed by the formation of a new peak at 980 cm^{-1} and 2980 cm^{-1}, demonstrating the presence of $-SO_3^-$ (NH_4^+) or $-SO_4^{2-}$ $(NH_4^+)_2$. [79]. It was worth mentioning that the ES-PANI/CFs presented excellent cycling performance with 82% capacity retention after 100 cycles at 5 A g^{-1}.

In general, various kinds of materials containing PBAs, metal-based compounds, and organic materials have been widely employed as cathodes for AIBs. The charge storage mechanism of these host materials is inseparable from the formation and rupture of hydrogen bonds with NH_4^+. Among them, PBAs with open-framework structure exhibit many merits such as simple synthesis, low cost, large enough diffusion channels to accommodate large-sized NH_4-ions, ultra-long lifespan and unexpected rate capability, and are very promising cathode materials for AIBs. At the same time, other kinds of cathode materials also need further attention and development to better meet the energy storage requirements of AIBs.

4. Anode materials for AIBs

Anode material is also a key factor for AIBs, because they require a relatively low potential to meet a high cell potential. It is also for this

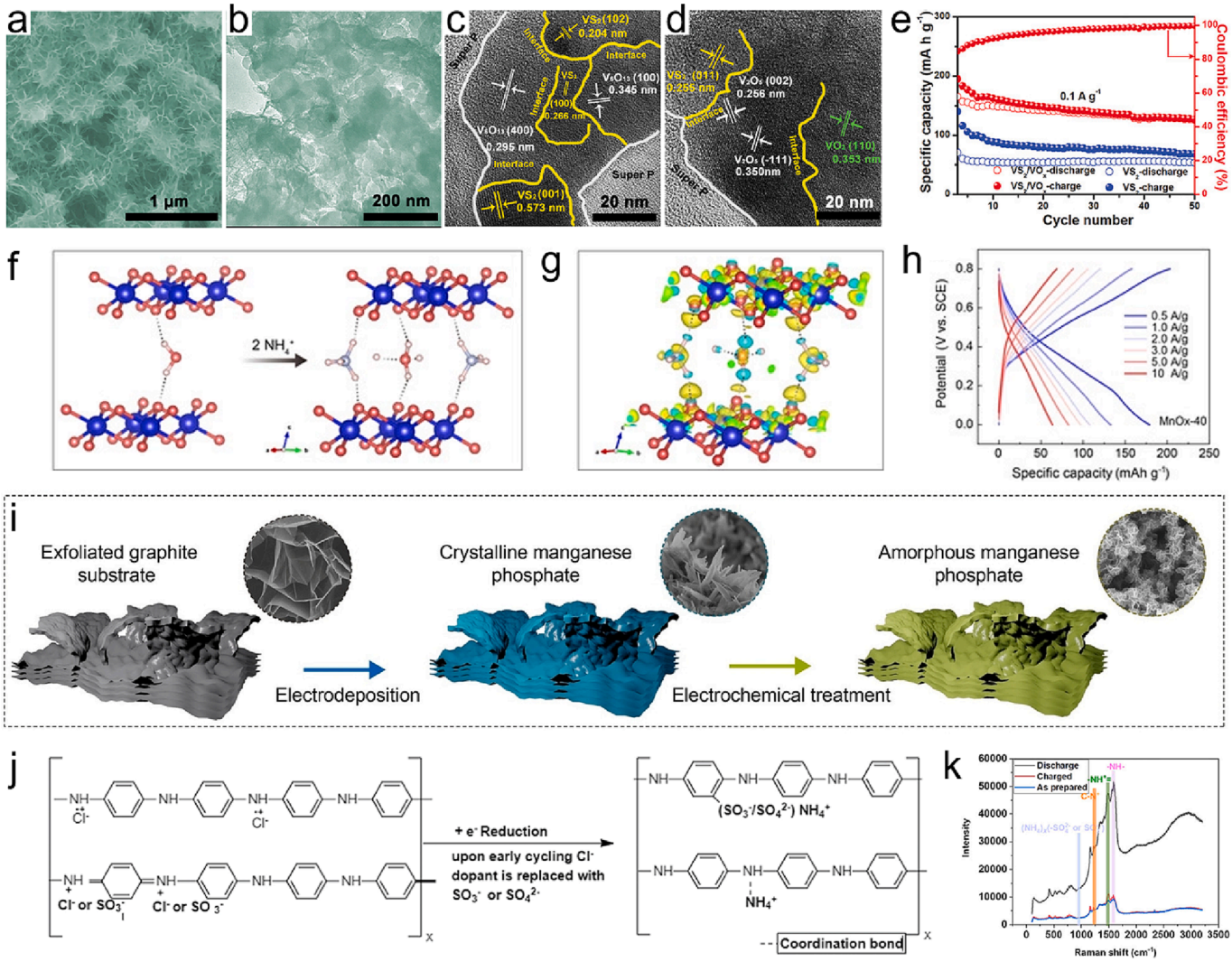

Fig. 5. (a–d) The morphology and microstructure of in situ formed VS_2/VO_x. (e) The comparison of cycling performance between VS_2/VO_x heterostructure electrode and VS_2 electrode in 5 m $(NH_4)_2SO_4$. (a–e) Reproduced with permission [27]. Copyright 2020, Wiley-VCH. (f) The lowest energy configuration of hydrous MnO_2 hosting NH_4^+. (g) Diagram of charge density difference of NH_4· inserted layered MnO_2 structure. (h) Galvanostatic charge/discharge curves of MnO_x-40 at different current densities. (f–h) Reproduced with permission [26]. Copyright 2020, Wiley-VCH. (i) Schematic illustration of the fabrication process for the manganese phosphate electrode. Reproduced with permission [78]. Copyright 2022, Wiley-VCH. (j) Reaction pathway; (k) Raman spectra of the ES-PANI electrodes at charged and discharge states. (j, k) Reproduced with permission [79]. Copyright 2020, American Chemical Society.

reason that anode materials are reported less than cathode materials. As listed in Table 2, we have summarized anode materials such as organic compounds, transition metal oxides and others, and their corresponding performance for AIBs. This section will introduce the performance of these common anode materials for AIBs and their NH4-ion storage mechanism.

Table 2
Summary of various anode materials and the corresponding performance for AIBs.

Materials	Electrolyte	Voltage range	Specific capacity (current density)	Cycling stability (cycles, current density)	Ref.
poly(1,5-NAPD)	19M CH_3COONH_4	−0.8–0.4 V vs. Ag/AgCl	141 mAh·g^{-1} (1 A·g^{-1})	94% (1000, 5 A g^{-1})	[54]
PTCDI	1M $(NH_4)_2SO_4$	−1.0–0.2 V vs. Ag/AgCl	105 mAh g^{-1} (1.2 A g^{-1})	89.5% (500, 1.2 A g^{-1})	[20]
PNTCDA	25 m NH_4Ac	−1.0–0 V vs. Ag/AgCl	106 mAh g^{-1} (8 A g^{-1})	88.7% (30 000, 8 A g^{-1})	[87]
CF@PANI	1M $(NH_4)_2SO_4$	−0.1–0.5 V vs. Ag/AgCl	77 mAh g^{-1} (0.1 A g^{-1})	81.8% (100, 0.1 A g^{-1})	[71]
QA-COF	0.5M $(NH_4)_2SO_4$	−0.6–0.6 V vs. SCE	220.4 mAh g^{-1} (0.5 A g^{-1})	90.7% (500, 0.5 A g^{-1})	[25]
ALO	1M $(NH_4)_2SO_4$	−0.8–0.1 V vs. Ag/AgCl	120 mAh g^{-1} (10 A g^{-1})	80% (1500, 10 A g^{-1})	[90]
$TiO_{1.85}(OH)_{0.30}·0.28H_2O$	25 m NH_4Ac	−1.3–−0.6 V vs. Ag/AgCl	84 mAh g^{-1} (0.5 A g^{-1})	80% (125, 5 A g^{-1})	[92]
h-MoO_3	1M NH_4Cl	−0.5–0.8 V vs. SCE	115 mAh g^{-1} (0.1 A g^{-1})	94% (100 000, 15 A g^{-1})	[94]
h-WO_3	1M $(NH_4)_2SO_4$	−1.1–0.8 V vs. Ag/AgCl	82 mAh g^{-1} (1 A g^{-1})	68% (200 000, 20 A g^{-1})	[95]
VO_x@PPy	0.5M NH_4Ac	−0.9–0 V vs. SCE	195.4 mAh g^{-1} (0.2 A g^{-1})	85% (2000, 1 A g^{-1})	[96]
d-VO	1M $(NH_4)_2SO_4$	−0.7–0.3 V vs. Ag/AgCl	200 mAh g^{-1} (0.1 A g^{-1})	72.9% (1000, 2 A g^{-1})	[23]
$K_{0.38}(H_2O)_{0.82}MoS_2$	1M $(NH_4)_2SO_4$	−0.4–0.8 V vs. Ag/AgCl	50.7 mAh g^{-1} (0.5 A g^{-1})	72% (50, 0.5 A g^{-1})	[100]

Note: poly(1,5-NAPD), poly(1,5-naphthalenediamine); PTCDI, 3,4,9,10-perylenetetracarboxylic diimide; PNTCDA, 1,4,5,8-naphthalenetetracarboxylic dianhydride-derived polyimide; COF, covalent organic framework; ALO, alloxazine; VO_x@PPy, vanadium oxide/polypyrrole; d-VO, defective VO_2; KMS, $K_{0.38}(H_2O)_{0.82}MoS_2$.

4.1. Organic compounds

Organic compounds with flexible structures and large internal voids are used not only as cathodes but also more as anodes for AIBs [54,58]. Particularly, the NH_4-ion storage mechanism in organic anode materials containing C=O bonds is propounded, which can accommodate NH_4 by the reaction of NH_4-ions with C=O bonds [32]. For instance, PTCDI with high capacity has been used as cathode for Li/Na-ion batteries [83,84]. Its inherent characteristics of π–π aromatic stacking make it have high electron transfer [85], which also makes it a potential anode for AIBs. In Ji's study, PTCDI has been demonstrated to have an attractive performance for NH_4^+ storage [20]. At 0.24 A g^{-1}, a maximum reversible capacity of 127.9 mAh g^{-1} with two reversible charge/discharge plateaus was observed in Fig. 6a, indicating the incorporation of two NH_4^+. Specifically, Fig. 6b depicted the mechanism for NH_4^+ insertion in PTCDI anode. The C=O bond in carbonyl groups located at diagonal position in the PTCDI structure would be broken to form O−NH_4^+ [20]. Polyimide (PI or PNTCDA) also attracted attention as an appealing electrode material for rechargeable batteries [86]. Later, the above group investigated NH_4^+ insertion of the PNTCDA anode in 25 m NH_4Ac water-in-salt electrolytes [87]. As shown in Fig. 6c and d, this anode delivered an excellent rate capability (a capacity of 80 mAh g^{-1} even at 100 C) and a remarkable cycling stability (capacity maintained at 88.7% even over 30 000 cycles at 50 C). Also, the NH_4^+ storage mechanism of PNTCDA was demonstrated to be similar to PTCDI (Fig. 6e). Moreover, Li et al. and Wang's group both fabricated the flexible full AIBs by employing ammonium vanadate cathode and PANI anode, which exhibited remarkable flexibility and excellent electrochemical performance at different bending angles [71,72]. Their works shed a light on developing flexible aqueous AIBs in the future.

Covalent organic frameworks (COFs) with an open channel for the transport of ions/electrons and the facilitated infusion of electrolyte can serve as potential electrode materials [88]. Currently, a COF anode reported by Alshareef et al. could achieve a high capacity of 220.4 mAh g^{-1} at 0.5 A g^{-1}, outperforming previous reported [25]. Thereafter, the intercalation mechanism of NH_4^+ ions in this COF electrodes was also explored by combining spectroscopic analysis and theoretical simulations, confirming H-bonds between NH_4^+ and COFs. Alloxazine (ALO), having high theoretical specific capacity of 250 mAh g^{-1}, outstanding cycling stability, excellent rate performance, together with low redox potential, is another attractive organic anode material [89,90]. Most recently, Tao et al. introduced the ALO anode for aqueous AIBs, achieving a capacity of 120 mAh g^{-1} at 10 A g^{-1} because of its pseudocapacitive effect along with rapid diffusion kinetics of NH_4^+ (Fig. 6f). Meanwhile, a full cell assembled with Ni-APW cathode and ALO anode could maintain a capacity of 110 mAh g^{-1} at 5 A g^{-1} over 10 000 cycles, and the Coulombic efficiency was always stable at 100% (Fig. 6g) [90].

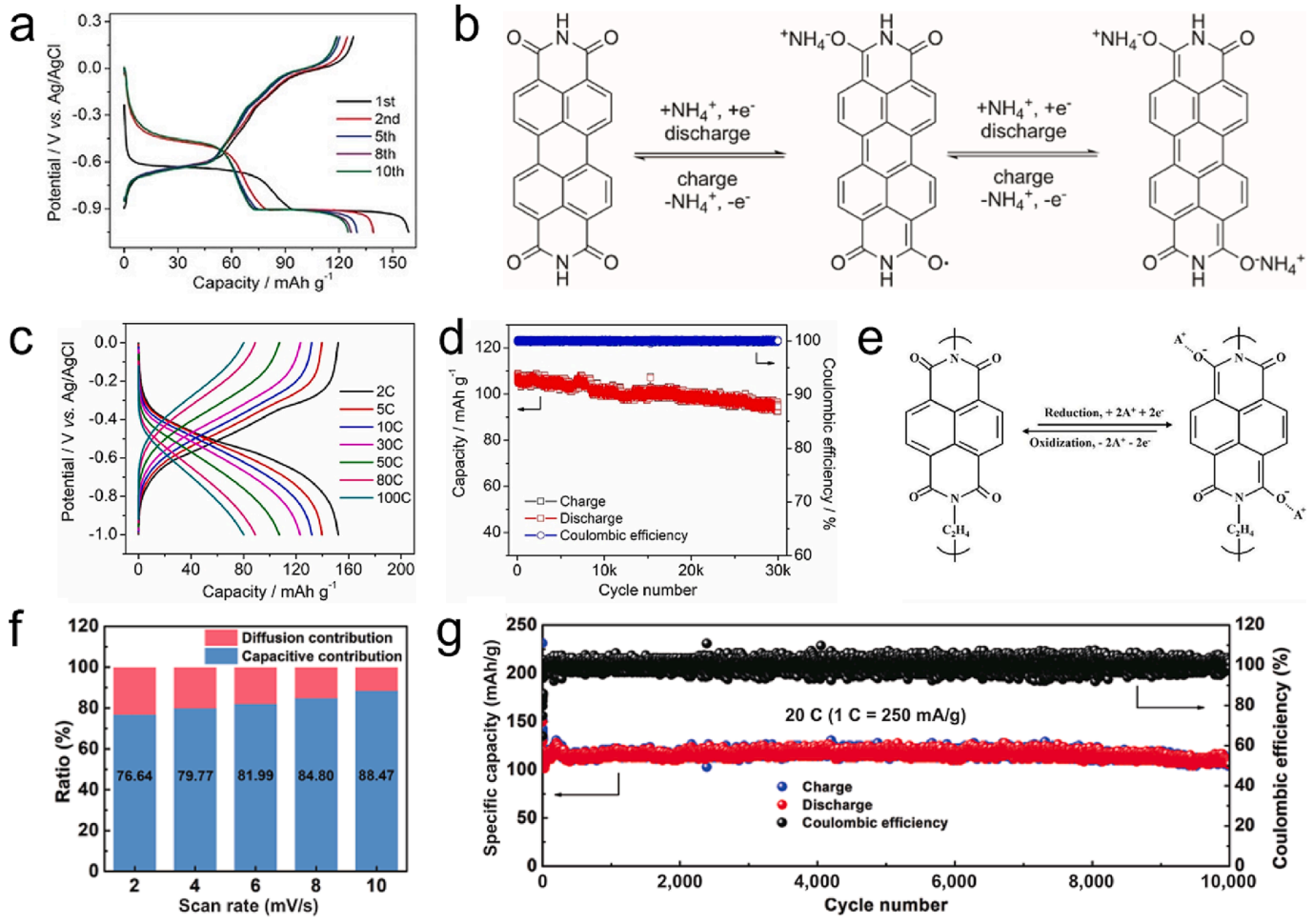

Fig. 6. (a) GCD profiles at 240 mA g^{-1}; (b) NH_4^+-ion intercalation mechanism of PTCDI anode. (a, b) Reproduced with permission [20]. Copyright 2017, Wiley-VCH. (c) Rate performance; (d) Cycling performance at 50 C; (e) Scheme of the A^+ (NH_4^+) storage mechanism of PNTCDA. (c-e) Reproduced with permission [87]. Copyright 2020, Elsevier. (f) Bar chart showing the percentage of the pseudocapacitive contribution at different scan rates of ALO anode. (g) Cycling performance of full battery at 20 C. (f, g) Reproduced with permission [90]. Copyright 2021, Springer Nature.

4.2. Transition metal oxides

It is common knowledge that transition metal oxides (TMOs) are extensively used as anode materials for aqueous batteries owing to their high capacity and low potential [91]. This experience is no exception for aqueous AIBs. In 2018, amorphous titanic acid ($TiO_{1.85}(OH)_{0.30}{\cdot}0.28H_2O$) was reported as anode host for NH_4^+ [92]. It was confirmed by *ex-situ* FTIR that a strong NH_4^+–O–Ti H-bond between $NH_4^+$and the titanic acid was formed. Specifically, after the ammoniation of the titanic acid at − 1.3 V vs. Ag/AgCl, the broad Ti–O bond peak of 1550 ~ 1600 cm^{-1} showed an obvious red-shift [92]. Molybdenum oxides are also very competitive candidates for aqueous battery assembly due to their low cost and specific tunnel structure [93]. In 2020, Zhi's group reported a hexagonal MoO_3 (h-MoO_3) electrode (Fig. 7a), whose large hosting spatial location is beneficial for cations migration [94]. As a result, h-MoO_3 could provide a decent capacity of 32 mAh g^{-1} even at 15 A g^{-1} and maintain 94% capacity after 100 000 cycles. Such excellent performance should be attributed to the ultrafast battery kinetics, originating from the reversible building/breaking of H-bonds between NH_4^+ and the exposed corner O in h-MoO_3 (Fig. 7b) [94]. With similar structure, h-WO_3 maintains high structural stability, which can be confirmed by SEM observation (Fig. 7c) that the overall morphology of h-WO_3 has not changed during charge–discharge [95]. This is because NH_4^+ ions can pass through the ionic channel and be easily accommodated in it, leading to great stability of up to 200 000 cycles with 68% capacity retention at 20 A g^{-1} [95]. Additionally, the simulated

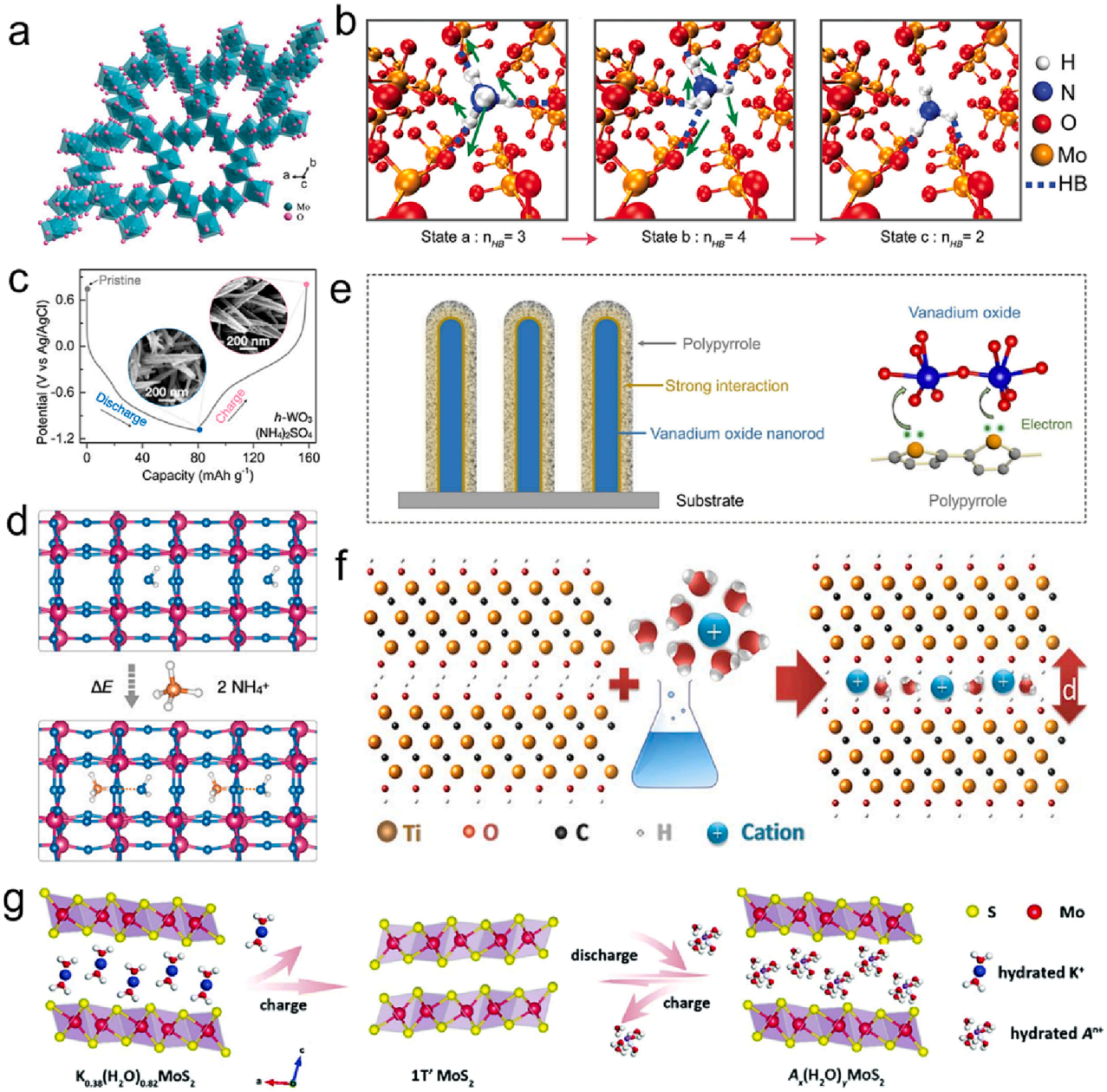

Fig. 7. (a) Tunnel structure of h-MoO_3. (b) Evolution of three stages during NH_4^+ diffusion process from state a to b to c. (a, b) Reproduced with permission [94]. Copyright 2020, Wiley-VCH. (c) Charge–discharge profile of h-WO_3. (d) The lowest-energy configuration of h-WO_3 with intercalated NH_4^+ ions. (c, d) Reproduced with permission [95]. Copyright 2022, Wiley-VCH. (e) Schematic illustration of the interaction between PPy and VO_x. Reproduced with permission [96]. Copyright 2022, Elsevier. (f) Schematic illustration of the intercalation of cations between $Ti_3C_2T_x$ layers. Reproduced with permission [99]. Copyright 2013, Science. (g) Schematic diagrams illustrating the charge storage mechanism of hydrated cations in bulk $K_{0.38}(H_2O)_{0.82}MoS_2$. Reproduced with permission [100]. Copyright 2020, The Royal Society of Chemistry.

intercalation process of NH_4^+ ions into h-WO_3 tunnels was also uncovered. It can be seen from Fig. 7d that the inserted NH_4^+ interacts with not only h-WO_3 but also the adjacent H_2O through hydrogen bonds [95]. More recently, Liu and coworkers fabricated an electrodeposited vanadium oxide/polypyrrole (VO_x@PPy) anode [96]. Thanks to the strong interaction between PPy and VO_x (Fig. 7e), this anode delivered a high specific capacity of 195.36 mAh g^{-1} at 0.2 A g^{-1} (superior to previous reported anode materials in NH_4^+ storage) [96]. Besides, defective VO_2 was evaluated as a high-capacity (about 200 mAh g^{-1} at 0.1 A g^{-1}) anode material for aqueous AIBs, which broadened the potential application of this battery for sustainable energy storage [23].

4.3. Others

In addition to organic compounds and TMOs, other metal-based materials like MXenes and transition metal sulfides as anode materials have gradually aroused researchers' interests [97,98]. MXenes are a large family of two-dimensional (2D) materials with good electrical conductivity and hydrophilic surfaces [99]. As early as 2013, Gogotsi's group reported spontaneous intercalation behavior of NH_4-ions between 2D $Ti_3C_2T_x$ MXene layers (Fig. 7f), but it showed charge storage properties more like capacitive behavior [99]. In another study, a hydrated-based molybdenum sulfide $K_{0.38}(H_2O)_{0.82}MoS_2$ (KMS) was proposed by Huang et al., who utilized it as a common host to act as an anode for various rechargeable aqueous cation (K^+, Na^+, Li^+, NH_4^+, Mg^{2+}, Al^{3+}, *etc.*) batteries [100]. It could achieve a stable redox potential of about −0.1 V vs. Ag/AgCl and a larger interlayer spacing with a higher specific capacity of over 50 mAh g^{-1} at 0.5 A g^{-1} compared to MoS_2. Therefore, interlayer engineering can be an effective method to enlarge the interlayer spacing, thus promoting the NH_4^+ storage capability for layered compounds in AIBs. Fig. 7g depicted the charge–discharge process of KMS. Obviously, it experienced a two-phase reaction [100]:

$$K_{0.38}(H_2O)_{0.82}MoS_2 – 0.38e^- \rightarrow MoS_2 + 0.38K^+ \quad (5)$$

$$MoS_2 + xA(H_2O)_y^{n+} + xe^- \leftrightarrow A_x(H_2O)_yMoS_2 (A=K,Na,Li,NH_4,Mg,Al) \quad (6)$$

It is worth noting that the topological chemistry of reversible (de) intercalation cations in MoS_2 relies on the composition of electrolyte during the subsequent discharge and charge [100].

In summary, various anode materials including organic compounds, metal oxides/sulfides have been reported. Like cathode materials, their NH_4^+ storage mechanism is also related to the formation/fracture of H-bonds. Among them, organic compounds are widely explored as anodes of AIBs due to their abundant resources, wide redox potential and easy recycling. Although these anode host materials have achieved good performance, their lower potential makes it more difficult to study anode materials compared with cathode materials. As an indispensable part of the battery, the importance of anode is self-evident. Therefore, other better anode materials are also worthy of researchers' attention.

5. Other energy-storage devices

Although AIB has obvious advantages, its research is still in the initial stage, and there are still several challenges such as low working potential and low energy density that need to be further solved. As a result, it is necessary to explore other high-performance energy storage devices to alleviate these issues. Undoubtedly, electrode materials are still the research focus of these devices. We have summarized the electrode materials and corresponding performance of these NH_4^+ storage devices, as shown in Table 3. This section will introduce the electrode materials used in other ammonium ion energy storage devices such as NH4-ion supercapacitors, NH4-ion capacitors, ammonium dual-ion batteries, and ammonium-zinc hybrid batteries and their ammonium-ion storage mechanism in addition to aqueous ammonium-ion batteries.

Table 3
Summary of various electrode materials and the corresponding performance for other NH_4^+ storage devices.

Electrode type	Devices	Materials	Electrolyte	Voltage range	Specific capacity (current density)	Cycling stability (cycles, current density)	Ref.
Cathodes	NH_4^+-SCs	PVO	1M PVA/NH_4Cl	−0.2–1.0 V vs. Ag/AgCl	351F·g^{-1} (1 A·g^{-1})	82% (2000, 1 A g^{-1})	[106]
		NVO	1M PVA/NH_4Cl	−0.8–1.0 V vs. Ag/AgCl	339F·g^{-1} (0.5 A·g^{-1})	71% (14 000, 100 mV s^{-1})	[101]
		VOH/PEDOT	1M PVA/NH_4Cl	−0.2–1.0 V vs. Ag/AgCl	327F g^{-1} (0.5 A g^{-1})	47% (6000, 1 mV s^{-1})	[103]
		ACC@VPP	1M PVA/NH_4Cl	−0.5–1.0 V vs. Ag/AgCl	511F g^{-1} (0.5 A g^{-1})	72% (10 000, 0.5 A g^{-1})	[102]
		δ-MnO_2	1M $(NH_4)_2SO_4$	0–1.0 V vs. SCE	9.5F cm^{-2} (2 mA cm^{-2})	60% (5000, 20 mA cm^{-2})	[28]
		P-M−S	27 m NH_4Ac	−1.0–0.1 V vs. Ag/AgCl	196F g^{-1} (1 A g^{-1})	—	[110]
	ADIBs	$Na_2Fe[Fe(CN)_6]$	Na_2SO_4/$(NH_4)_2SO_4$	−0.2–1.4 V vs. SHE	77 mAh g^{-1} (0.1 A g^{-1})	53% (600, 0.5 A g^{-1})	[44]
		PTMA	1M $(NH_4)_2SO_4$	0.1–1.0 V vs. SCE	80 mAh g^{-1} (0.5 A g^{-1})	86.4% (10 000, 5 A g^{-1})	[117]
		PANI/CNF	1M $(NH_4)_2SO_4$	0.1–1.0 V vs. SCE	212.5 mAh g^{-1} (0.5 A g^{-1})	72.1% (5000, 5 A g^{-1})	[118]
	AHBs	Na-FeHCF	$ZnSO_4$/$(NH_4)_2SO_4$	−0.2–0.7 V vs. SCE	67.4 mAh g^{-1} (0.5 A g^{-1})	92.1% (2000, 2 A g^{-1})	[120]
		CuHCF	1M $(NH_4)_2SO_4$	0.3–1.1 V vs. SCE	58.8 mAh g^{-1} (0.3 A g^{-1})	78.4% (1000, 1.8 A g^{-1})	[121]
		A-NiCo-DH	2M NH_4Ac	0–0.9 V vs. SCE	280.6 mAh g^{-1} (0.72 A g^{-1})	72.1% (1000, 7.2 A g^{-1})	[31]
Anodes	NH_4^+-SCs	$(NH_4)_xWO_3$	2M NH_4Ac	−0.8–0.2 V vs. SCE	8.0F cm^{-2} (2 mA cm^{-2})	85.8% (5000, 20 mA cm^{-2})	[111]
		MoO_3@C	$(NH_4)_2SO_4$-gel	−0.6–0.6 V vs. Ag/AgCl	473F·g^{-1} (1 A·g^{-1})	92.7% (5000, 20 A g^{-1})	[112]
		MoS_2@TiN/CNTF	1M NH_4Cl	−0.8–0 V vs. Ag/AgCl	1.1F cm^{-2} (2 mA cm^{-2})	—	[113]
	AICs	rGO-PI	$(NH_4)_2SO_4$-gel	−1.0–0 V vs. SCE	102F·g^{-1} (0.5 A·g^{-1})	94.2% (10 000, 5 A g^{-1})	[29]
	ADIBs	PI	1M $(NH_4)_2SO_4$	−0.9–0.1 V vs. SCE	157.3 mAh g^{-1} (0.5 A g^{-1})	—	[117]
		PI/NDC/CNT	1M $(NH_4)_2SO_4$	−0.9–0.1 V vs. SCE	161 mAh g^{-1} (0.5 A g^{-1})	87.9% (5000, 0.5 A g^{-1})	[118]
		PTCDI	1m NH_4PF_6/ADN-EMC	−1.0–0.4 V vs. SHE	67 mAh g^{-1} (0.08 A g^{-1})	—	[30]

Note: SCs, supercapacitors; ADIBs, ammonium dual-ion batteries; AHBs, ammonium-zinc hybrid batteries; AICs, NH_4-ion capacitors; PVA, polyvinyl alcohol; NVO, $(NH_4)_2V_{10}O_{25}·8H_2O$; VOH/PEDOT, poly(3,4-ethylenedioxithiophene) (PEDOT) intercalated hydrated vanadium oxide (VOH); ACC@VPP, PEDOT/PSS intercalated VOH on active carbon cloth (ACC); PTMA, poly(2,2,6,6-tetramethylpiperidinyloxy-4-yl methacrylate); CNF, carbon nanofiber; A-NiCo-DH, activated NiCo double hydroxide; MoS_2@TiN/CNTF, MoS_2 nanosheets anchored on TiN nanowires supported on carbon nanotube fibers; rGO-PI, graphene-polyimide; NDC, nitrogen-doped carbon; NH_4PF_6/ADN-EMC, ammonium hexafluorophosphate/adiponitrile-ethyl methyl carbonate.

5.1. Supercapacitors

At present, most researches about NH_4^+-storage electrode materials focus on aqueous AIBs. However, there is a rare research on NH_4-ion supercapacitors (SCs) [101–103]. It is well-known that NH_4-ion SCs are energy storage devices between NH_4-ion capacitors and NH_4-ion batteries with special properties such as higher capacity, longer cycle life and shorter charge/discharge time than NH_4-ion capacitors, and their electrochemical performance mainly depends on electrode materials [104,105]. Therefore, it is necessary to explore advanced electrode materials for NH_4^+-SCs.

Layered vanadium oxides and their derivatives as electrode materials can be used not only for AIBs but also for NH_4^+-SCs because of V multiple valances and adjustable structure to effectively insert/extract ions [106]. For instance, Wang et al. synthesized an ammonium vanadium oxide framework of $(NH_4)_2V_{10}O_{25}{\cdot}8H_2O$ (NVO) for flexible quasi-solid-state (FQSS) hybrid SC (HSC) by hydrothermal route (Fig. 8a) [101]. HSC often has the advantage of large potential window [107]. The NVO cathode manifested a remarkable capacity (169 mAh g^{-1} at 0.5 A g^{-1}) in NH_4Cl/PVA electrolyte, outperforming the value in NH_4Cl electrolyte (134 mAh g^{-1}). From Fig. 8b, we can see that the CV curves exhibited a rectangle-like shape with two couples of broad peaks and they became inconspicuous due to the decrease of NH_4^+ intercalation and H-bond contribution when scan rete up to 100 mV s^{-1}, which indicates that the storage mechanism of NVO belongs to both the double layer capacitance and intercalation pseudocapacitance [101]. To enhance the kinetics and stabilize the structure during the NH_4^+ (de)intercalation, their group proposed PVO with the expanded interlamellar spacing of 13.9 Å [106]. The FQSS PVO//AC HSC showed outstanding cycle stability with ca. 60% over 10 000 cycles (Fig. 8c). Later, Chen et al. of the same group

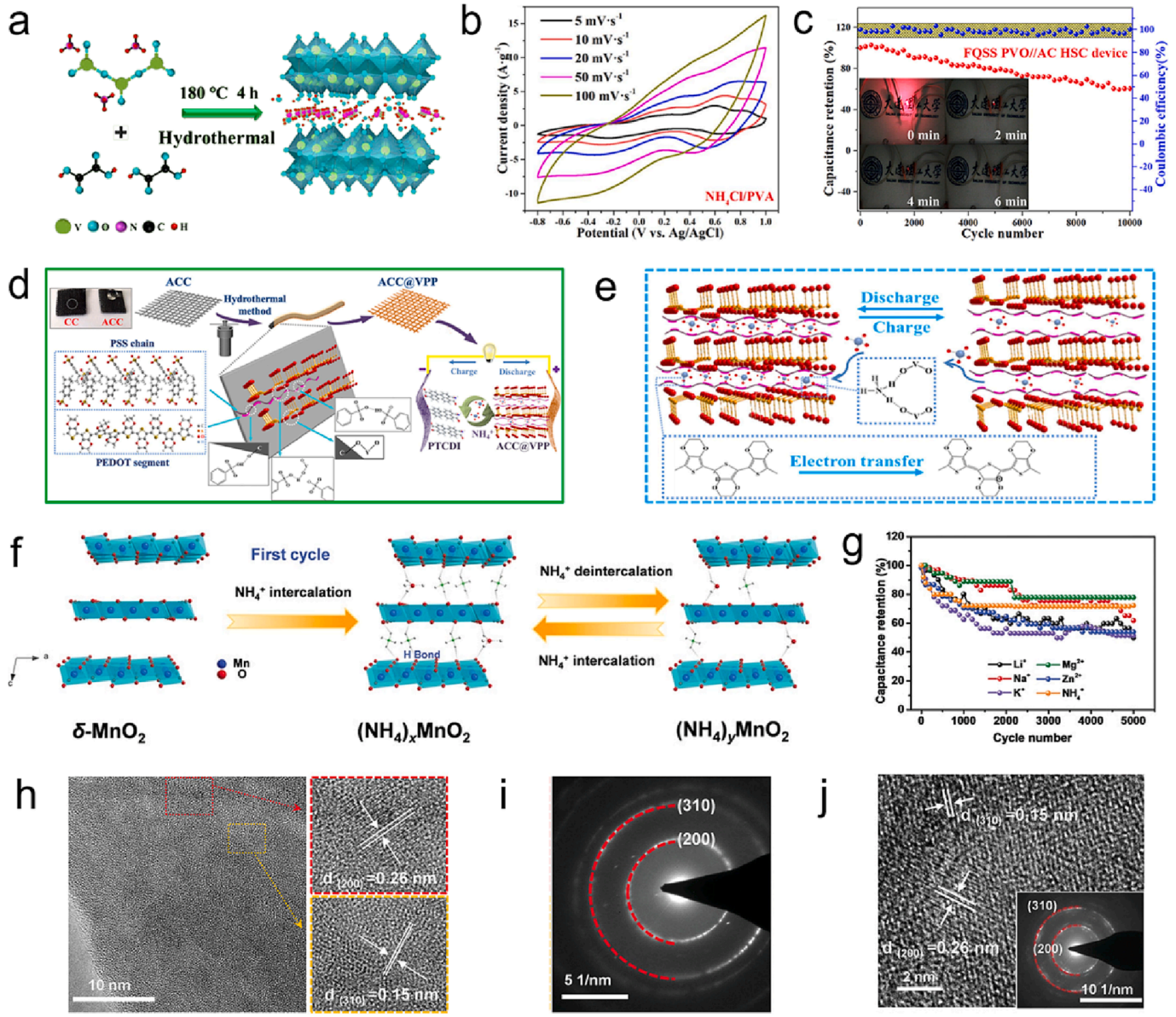

Fig. 8. (a) Schematic diagram of the concise synthetic strategy of NVO nanosheets. (c) CV curves of NVO at various scan rates in NH_4Cl/PVA electrolyte. (a, b) Reproduced with permission [101]. Copyright 2021, Elsevier. (c) Cycle performance of the FQSS PVO//AC HSC device. Reproduced with permission [106]. Copyright 2021, Elsevier. (d) Flow diagrams of the synthesis and formation mechanism; (e) Schematic illustration of NH_4^+-storage mechanism of ACC@VPP electrode for flexible NH_4^+-SCs. (d, e) Reproduced with permission [102]. Copyright 2022, Elsevier. (f) Schematic illustration of the ammonium-ion storage mechanism in the layered δ-MnO_2. (g) Cycling performance of the MnO_2//ACC HSCs. (h) HRTEM images and (i) SAED pattern of the pristine δ-MnO_2. (j) HRTEM (inset: SAED pattern) of the discharged δ-MnO_2. (f-j) Reproduced with permission [28]. Copyright 2022, Wiley-VCH.

successively developed VOH/PEDOT (hydrated vanadium oxide/poly (3,4-ethylenedioxithiophene)) [103] and ACC@VPP (PEDOT/PSS intercalated VOH on active carbon cloth (ACC)) (Fig. 8d) [102] as host materials for NH_4^+-HSC. The NH_4^+-storage mechanism in the ACC@VPP electrode is shown in Fig. 8e, in which the reversible (de)intercalation of NH_4^+ is accompanied by H-bonds construction/rupture between NH_4^+ and V–O layers [102]. The reaction mechanism can be described by the following equation:

$$(NH_4)_mV_2O_5 \rightleftarrows (NH_4)_{m-x}V_2O_5 + xNH_4^+ + xe^- \quad (7)$$

The intercalant of polymer played an auxiliary role in the ion diffusion and electron transfer of electrode materials, which endowed ACC@VPP with a high superior capacitance of 170 mAh g^{-1} at 0.5 A g^{-1} [102].

Besides, MnO_2 has also gradually become a potential electrode material for SCs owing to its layered structure and considerable theoretical capacitance (1110 F g^{-1}) [108,109]. In 2021, Zhou et al. assembled an aqueous ammonium-ion HSC (A-HSC) based on the layered δ-MnO_2 cathode, ACC anode, and aqueous $(NH_4)_2SO_4$ electrolyte [28]. Similar to

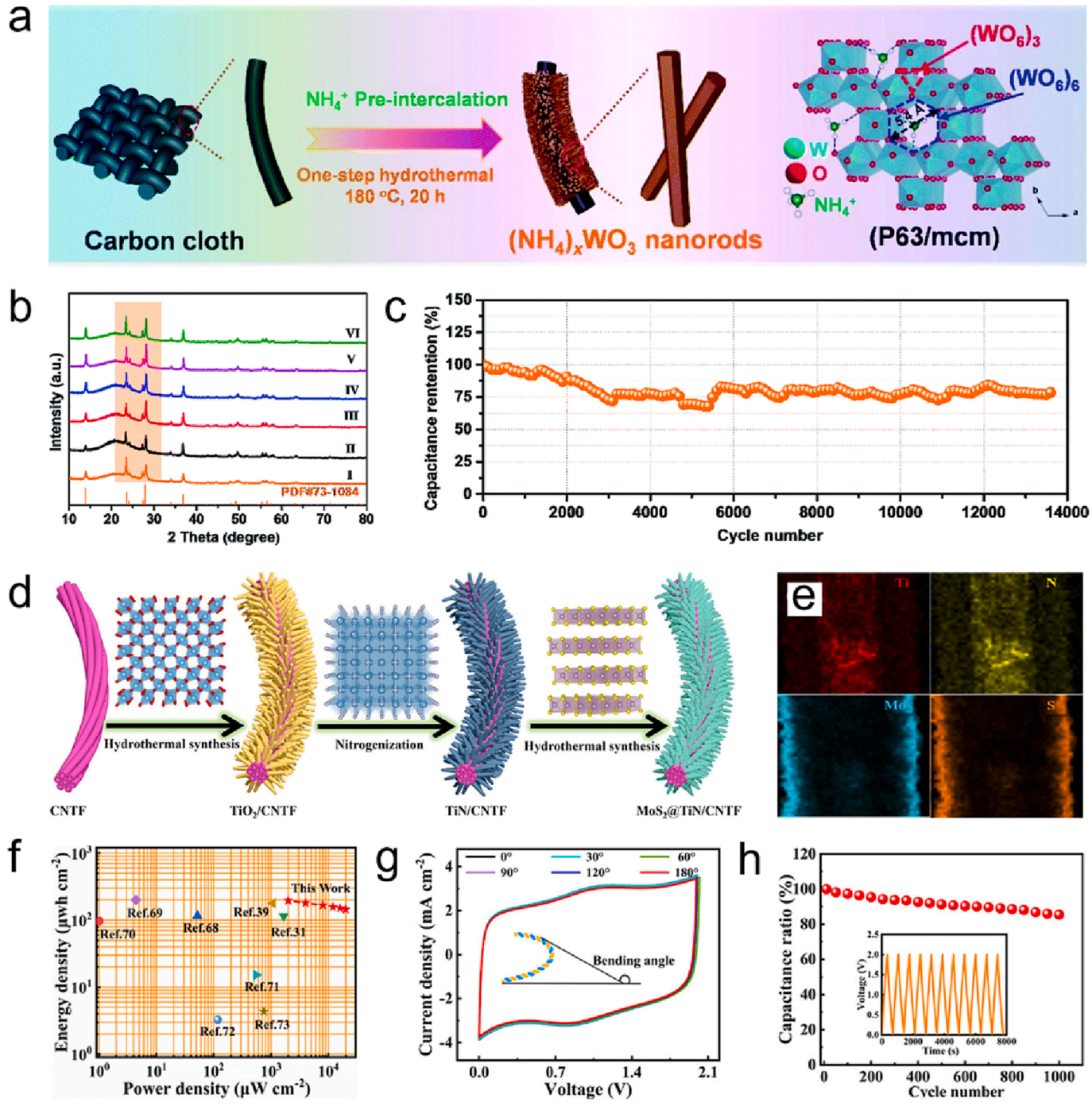

Fig. 9. (a) Schematic diagrams of the structure and synthesis process of $(NH_4)_xWO_3$. (b) The ex situ XRD patterns of $(NH_4)_xWO_3$ anode. (c) Cycling performance (at 20 mA cm^{-2}) of $(NH_4)_xWO_3$//α-MnO_2 A-HSCs. (a-c) Reproduced with permission [55]. Copyright 2022, The Royal Society of Chemistry. (d) Schematic illustration of the synthetic process of MoS_2@TiN/CNTF. (e) EDS mappings of Ti, N, Mo, and S elements of MoS_2@TiN. (f) Ragone plots of the FAASC in this work and recently reported fiber-shape supercapacitors. (g) CV curves of the as-assembled FAASCs under various bending angles at 10 mV s^{-1}. (h) Cycling performance of the as-assembled FAASCs at 2 mA cm^{-2}. (d-h) Reproduced with permission [113]. Copyright 2022, American Chemical Society.

other TMOs, the NH_4^+ (de)intercalation in δ-MnO_2 cathode is also along with H-bond building/breaking (Fig. 8f). Compared with traditional aqueous metal-ion (K^+, Na^+, Li^+, Zn^{2+}) HSCs, A-HSCs delivered impressive cycling performance with 72.2% capacitance retention over 5000 cycles (Fig. 8g). It is impressive that the HRTEM image and SAED pattern (Fig. 8j) of the discharged δ-MnO_2 are almost identical to that of the pristine δ-MnO_2 (Fig. 8h and i), implying that the structural changes of δ-MnO_2 are negligible during the charging-discharging process, which may be attributed to the large amount of NH_4^+ ions inserted into the layered δ-MnO_2 as pillars to stabilize the structure [28]. Additionally, in order to efficiently suppress the dissolution and collapse of vanadium oxide and thus improve the cycling stability during charge/discharge, PPy coating or adding PVA to the electrolyte to form a hydration film coating electrode is also an effective strategy [96,101,106]. Furthermore, Lin and coworkers took the lead in applying organic polymers to ammonium-ion asymmetric SCs, which paved the way for future exploration in this direction [110].

Developing anode materials is more challenging than cathodes because of their lower potential. Therefore, A-SC anode materials reported in the literature are far less than cathodes. Most recently, Tang's group reported a tunnel-structured $(NH_4)_xWO_3$ anode (Fig. 9a) for fast NH_4^+ storage [111]. Coupled with α-MnO_2 cathode, a novel $(NH_4)_xWO_3$//α-MnO_2 A-HSC was developed. From *ex situ* XRD pattern (Fig. 9b), we can infer that the NH_4^+ (de)intercalation process is reversible, which is conducive to the cycling performance of A-HSCs, with capacity retention of 78.6% over 13 600 cycles (Fig. 9c). Another anode material MoO_3@C composite for NH_4^+-SCs delivered an unprecedented specific capacitance of 473 $F{\cdot}g^{-1}$ at 1 $A{\cdot}g^{-1}$ and 92.7% capacitance retention over 5000 cycles [112]. This excellent performance stems from the oxygen vacancies that enhance the ion/electron transport and electrochemical reaction sites of the composites, while promoting the formation of H-bonds between NH_4^+ and host materials [112]. Afterwards, freestanding core – shell heterostructure electrodes with MoS_2 nanosheets anchored on TiN nanowires supported on carbon nanotube fibers (MoS_2@TiN/CNTF) as anodes for fiber-shaped NH_4^+ asymmetric ASCs (FAASCs) were constructed by hydrothermal and nitridation methods (Fig. 9d and e) [113]. Ragone plots (Fig. 9f) depicted the areal energy density of FAASCs in this work dropped from 195.1 to 144.4 μWh cm^{-2} when the scan rate changed from 2 to 20 mA cm^{-2}, outperforming the most previously reported. In addition, the as-assembled FAASCs also showed good structural stability, outstanding mechanical flexibility and excellent cycling performances (Fig. 9g and h) [113].

5.2. NH_4-ion capacitors

Ion capacitor (IC) is a high-performance hybrid energy storage device, which can be made of the battery-type anode and EDLC-type cathode materials. Based on the advantages of wide working potential, great specific capacity and fast charge/discharge rates, IC can achieve extraordinary energy performance [114]. After Li-ion capacitor [115], Na-ion capacitor [116] or K-ion capacitor [114], NH_4-ion capacitors (AICs) show great prospect in energy storage.

Quite recently, Zhang et al. proposed an AIC by employing graphene-polyimide (rGO-PI) anode and N-doped carbon nanofiber (NCNF) cathode (Fig. 10a) [29]. Attributed to the unique microstructure and physiochemical characteristics of electrodes, as-assembled device displayed satisfying performances such as a high energy density of 45.9 Wh kg^{-1}, a good cycling stability of ~ 94% capacitance retention after 10 000 cycles at 5 A g^{-1} and good flexibility (Fig. 10b) [29]. However, there are few reports about AIC at present, which is worth further exploring.

5.3. Dual-ion battery

For the dual-ion battery (DIB), not only cations but also anions in electrolyte can be inserted. Specifically, it operates in a mode where

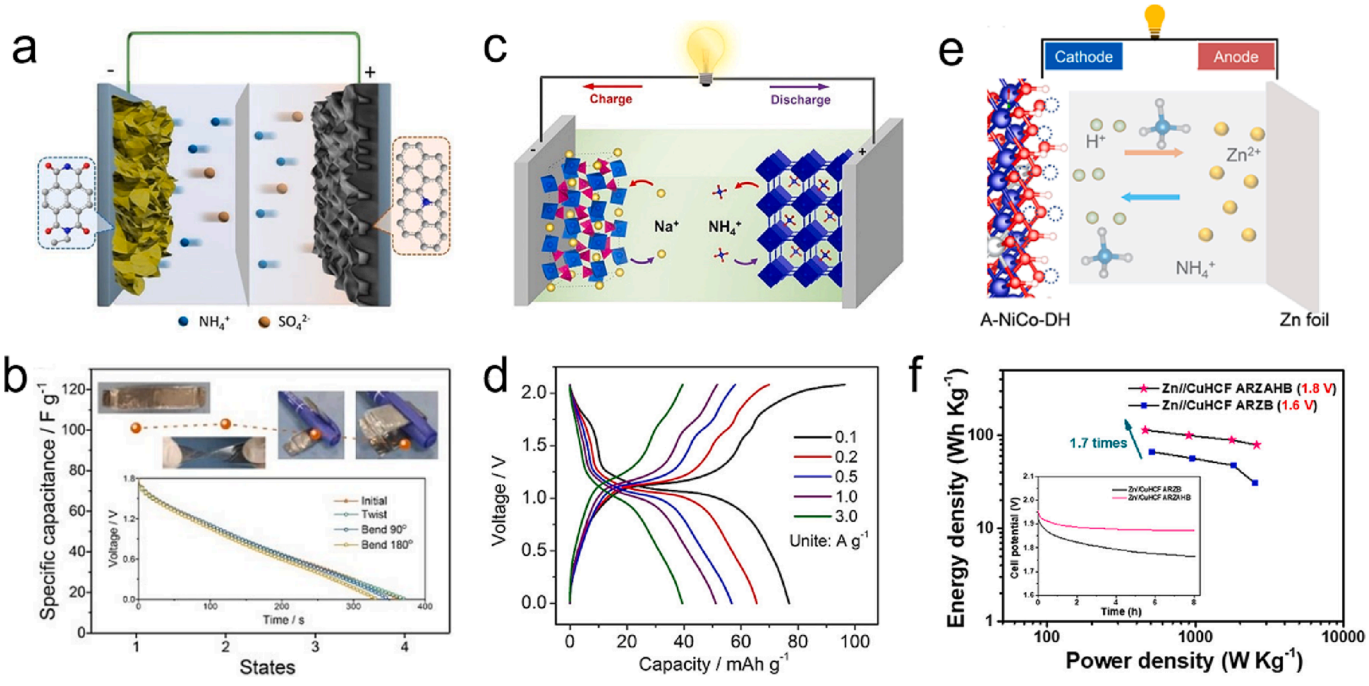

Fig. 10. (a) The diagrammatic sketch of electrochemical reaction mechanism. (b) Capacitance retention under of quasi-solid-state ammonium ion capacitor at various folding states (inset shows the corresponding discharge curves). (a, b) Reproduced with permission [29]. Copyright 2022, Wiley-VCH. (c) Schematic of the working mechanism of aqueous double-ion Na^+/NH_4^+ battery. (d) Rate performance, capacity, and current density based on the active mass of the cathode. (c, d) Reproduced with permission [44]. Copyright 2018, American Chemical Society. (e) Schematic illustration of the designed aqueous rechargeable ammonium-zinc hybrid battery (A-NiCo-DH//Zn). Reproduced with permission [31]. Copyright 2022, Springer Nature. (f) Ragone plots of Zn//CuHCF ARZAHB with comparison of Zn//CuHCF ARZB (inset is the open circuit voltage curve showing self-discharge behavior of two full cells). Reproduced with permission [121]. Copyright 2019, American Chemical Society.

cations are inserted into the anode and anions into the cathode, in which both cations and anions are charge carriers, alleviating the problem of low working voltage of AIBs (~1 V) [21].

Up to now, there are a few reports about the new ammonium dual-ion batteries (ADIBs). For example, Ji et al. constructed a DIB based on the $Na_2Fe[Fe(CN)_6]$ cathode hosting NH_4^+ and the $NaTi_2(PO_4)_3$ anode accommodating Na^+ during operation (Fig. 10c) by taking advantage of a higher working potential (~1.1 V) of NH_4^+ (de)insertion in the PBA's framework [44]. As shown in Fig. 10d, such a new system exhibited a promising rate capability. Meanwhile, the corresponding reaction equations of cathode were given as follows [44]:

$$Na_2Fe[Fe(CN)_6] \rightarrow Fe[Fe(CN)_6] + 2Na^+ + 2e^- \quad (8)$$

$$Fe[Fe(CN)_6] + NH_4^+ + e^- \leftrightarrow (NH_4)Fe[Fe(CN)_6] \quad (9)$$

In 2019, Zhang's group assembled an all-organic aqueous ADIB using the poly(2,2,6,6-tetramethylpiperidinyloxy-4-yl methacrylate) (PTMA) cathode (for reversible SO_4^{2-} insertion/extraction), PI anode (for reversible NH_4^+ (de)intercalation) and 1 M $(NH_4)_2SO_4$ aqueous electrolyte [117]. This ADIB demonstrated a wider working voltage (1.9 V) than typical aqueous AIBs [117]. Similarly, another purely organic ADIB consisting of PANI cathode and PI, N-doped carbon and carbon nanotubes anode could obtain a high energy density of 114.3 Wh kg^{-1} when the power density reached 18.6 kW kg^{-1} [118]. In 2022, Alshareef and coworkers proposed an ADIB with a record-breaking operation voltage of 2.75 V, suggesting the possibility of developing high-voltage AIBs to meet the sustainability requirements [30].

5.4. Hybrid battery

As a distinction, dual-cation batteries use only two cations as charge carriers, while hybrid batteries can use two or more cations as charge carriers, which can further expand the operating window and increase energy density [119]. At present, some researchers have combined AIBs with traditional metal-ion batteries like Zn-ion batteries to construct ammonium-zinc hybrid batteries (AHBs) to boost the feasibility and efficiency of AIBs in practical application. In 2019, Huang et al. fabricated such an AHB using Na-FeHCF nanocubes cathode for hosting NH_4^+ coupling with zinc anode [120]. This new hybrid battery displayed an operating voltage of 1.3 V and a decent energy density of 81.7 Wh kg^{-1}, outperforming many typical AIBs and hybrid batteries. Besides, the electrochemical mechanism of this battery could be represented as follows [120]:

Anode:

$$xZn \leftrightarrow xZn^{2+} + 2xe^- (0 \le x \le 0.5) \quad (10)$$

Cathode:

$$2xNa_{1.45}Fe^{III}[Fe^{II}(CN)_6]_{0.93}\cdot 3.2H_2O + 2xNH_4^+ + 2xe^- \leftrightarrow 2xNa_{1.45}(NH_4)Fe^{II}[Fe^{II}(CN)_6]_{0.93}\cdot 3.2H_2O \quad (11)$$

In another study of their group, only the cathode of AHB was replaced by CuHCF, and its working potential was increased to 1.8 V as well as a satisfactory energy density of 114 Wh kg^{-1} was obtained (Fig. 10f) [121]. Despite the increased energy density, their experiments encountered the problem of low capacity because only one redox pair was present during NH_4^+ insertion. Therefore, PBAs with multiple redox pairs are promising alternatives. Recently, Liu's group reported an electrochemically activated NiCo double hydroxide (A-NiCo-DH) as the cathode for aqueous AHB (Fig. 10e) [31]. This electrode delivered a high discharge capacity of 280.6 mAh·g^{-1} at 0.72 A·g^{-1}, which is attributed to the introduction of H vacancy in A-NiCo-DH during electrochemical activation, enhancing the electrochemical activity of the electrode material. Moreover, spectroscopy studies indicated that A-NiCo-DH experienced a NH_4^+/H^+ co-insertion mechanism and the electrochemical reactions are shown as follows [31]:

Anode:

$$Zn \leftrightarrow Zn^{2+} + 2e^- \quad (12)$$

Cathode:

$$NiCo_{4.1}H_{7.3}O_{10.3}(NO_3)_{0.28} + xNH_4^+ + yH^+ + (x+y)e^- \leftrightarrow NiCo_{4.1}(NH_4^+)_xH_{7.3+y}O_{10.3}(NO_3)_{0.28} \quad (13)$$

As mentioned above, similar to AIBs, the electrode materials of other devices used for NH_4^+ storage also include PBAs, metal-based compounds and organic materials. However, the research on these materials is still in its infancy, and the related reports are very limited, which needs more exploration. In view of the potential application of emerging NH_4-ion storage devices, it is necessary to take some structural strategies such as composites, doping and defect engineering to further optimize electrode materials to obtain better electrochemical performance.

6. Conclusions and perspectives

Emerging as a new class of large-scale electricity storage technologies, NH_4-ion storage devices including AIBs, AICs and NH_4^+-SCs have aroused researchers' great interest and have been considered as the most potential energy storage competitors owing to their abundant resources, inherent safety, fast diffusion capability and unique storage mechanism of NH_4^+. Finding suitable and efficient electrode materials for NH_4-ion storage devices with excellent electrochemical performance is still a huge challenge. This review focused on a wide range of cathode materials covering Prussian blue and its analogues, metal-based compounds, organic materials and anode materials including organic compounds, transition metal oxides and other anode compounds. Most importantly, the H-bond chemistry plays a significant role during NH_4-ion storage process, which brings new insights into the importance of chemical bonds between inserted ions and electrode hosts in high-power energy storage devices, and thus provides a new way to explore electrode design.

With respect to cathodes, PBAs are the most universal and potential cathode materials for NH_4-ion storage devices owing to the large interstitial sites and open channels in their framework structures. Although this kind of material has shown excellent electrochemical behaviors, its specific capacity is still limited and uncompetitive. Fortunately, the specific capacity of PBAs electrode can be improved by introducing the multivalent metals (for example V, Mn, Co, *etc.*) at the M' site to design the multi-pair redox. Therefore, PBAs electrode like VHCF, MnHCF and CoHCF should be more developed in the future research. Additionally, metal-based compounds (V-based and Mn-based) also possess the promising application prospect due to their considerable reversible capacity, but from the point of view of practical application, the stability of structure still needs to be improved. Inserting other particles (like Fe^{3+}, NH_4^+, PO_4^{3-}, PANI, *etc.*) into the metal layer is regarded as an effective strategy not only to enhance the cycling performance but also to further enhance the capacity of electrode materials. Furthermore, other structural strategies such as composites, doping and defect engineering are worthy of consideration. Another kind of very promising cathodes, organic materials, also exhibit great electrochemical performance with remarkable cycling stability. Nevertheless, few studies focus on the development of related materials, only PANI has been reported at present, and other types of organic materials need further exploration.

Regarding to the anode materials, organic compounds (PANI, PTCDI, *etc.*) have been regarded as the most potential anode for NH_4-ion storage devices due to their favorable performance. Such organic materials with multiple functional groups (such as C=O) which can well accommodate NH_4^+ at low potential are worthy of further development by researchers. However, organic compounds usually suffer from low electronic conductivity, which hinders their large-scale application. The preparation of organic composites with high conductivity can be achieved by coating

carbon-based materials such as CNT, Keqin Black, rGO, *etc*. Also, the cycling performance under low current density is still unsatisfactory, requiring extensive improvement. Other anode materials, such as h-MoO_3, h-WO_3, MXenes, *etc*. show excellent performance for NH_4-ion storage, but their output potential is high, so it is necessary to develop other metal-based materials with low output potential, such as titanium-based materials. Meanwhile, more experiments and simulations can be used in close conjunction to deeply understand how the physical and chemical properties of electrodes affect the electrochemical performance, so as to facilitate the development of electrodes. In general, however, the anode materials seem to have been relatively less studied compared with cathodes. As we know, as an indispensable part of EES devices, the anode is as important as cathode. As a result, NH_4-ion storage devices need to explore more novel electrode materials to meet all practical application requirements.

As for the ammonium-ion storage mechanism, we know that its exploration has a significant meaning in the fundamental understanding and future large-scale application of advanced ammonium-ion storage systems. There are two kinds of ammonium-ion storage mechanisms in various electrode materials, namely reversible insertion/extraction mechanism of NH_4^+ and adsorption mechanism of NH_4^+. The former is adopted for the energy storage mechanism of metal-based compounds, *i.e.*, the reversible insertion/extraction of NH_4^+ in the layers or tunnel structures of metal-based compounds, which is related to the formation/breakage of hydrogen bonds between NH_4^+ and metal-based compounds. While the latter mechanism is used for energy storage in organic materials, *i.e.*, NH_4^+ is mainly adsorbed on organic groups such as conjugated carbonyl groups and conjugated amine groups, and the hydrogen atoms in NH_4^+ form hydrogen bonds with oxygen or nitrogen atoms in organic compounds. However, the detailed ammonium-ion storage mechanism is difficult to be explained clearly because of the lack of reliable theoretical basis and advanced standard characterization techniques. Hence, developing more precise characterization techniques coupled with ab initio calculations will help to a better understanding of ammonium-ion storage mechanism and the correlation between the structure and property, which will provide fascinating guidelines to comprehend and design more efficient materials for NH_4-ion storage devices.

Even although some achievements have been made in electrode materials of NH_4-ion storage devices, it is still far from real practical application. There is still a lot of work to be done to advance the industrialization of NH_4-ion storage devices, such as the exploitation of novel cathode and anode materials with good rate capability and high conductivity, the optimization of electrolyte and additive, *etc*. In addition, there is another challenge that deserves our attention, *i.e.*, the safety of ammonium-ion storage devices, whose electrolyte is an ammonium salt solution, and NH_3 produced during energy storage can cause environmental pollution and health problems. Anyway, we firmly believe that the above solutions will eventually become a reality through unremitting scientific research, and as a strong competitor, NH_4-ion storage devices will have promising applications in large-scale stationary energy storage.

Declaration of Competing Interest

The authors declare that they have no known competing financial interests or personal relationships that could have appeared to influence the work reported in this paper.

Data availability

No data was used for the research described in the article.

Acknowledgements

This work was supported by the National Natural Science Foundation of China (No. 21676036) and the Graduate Research and Innovation Foundation of Chongqing (No. CYB22043 and CYS22073).

References

[1] Y. Wu, Y. Sun, Y. Tong, X. Liu, J. Zheng, D. Han, H. Li, L. Niu, Recent advances in potassium-ion hybrid capacitors: electrode materials, storage mechanisms and performance evaluation, Energy Stor. Mater. 41 (2021) 108–132, https://doi.org/10.1016/j.ensm.2021.05.045.
[2] S. Chu, Y. Cui, N. Liu, The path towards sustainable energy, Nat. Mater. 16 (2017) 16–22, https://doi.org/10.1038/nmat4834.
[3] R. Zhang, S. Wang, S. Chou, H. Jin, Research development on aqueous ammonium-ion batteries, Adv. Funct. Mater. 32 (2022) 2112179, https://doi.org/10.1002/adfm.202112179.
[4] G. Crabtree, Perspective: the energy-storage revolution, Nature 526 (2015) S92–S, https://doi.org/10.1038/526S92a.
[5] B. Dunn, H. Kamath, J.-M. Tarascon, Electrical energy storage for the grid: a battery of choices, Science 334 (2011) 928–935, https://doi.org/10.1126/science.1212741.
[6] X. Zeng, J. Hao, Z. Wang, J. Mao, Z. Guo, Recent progress and perspectives on aqueous Zn-based rechargeable batteries with mild aqueous electrolytes, Energy Stor. Mater. 20 (2019) 410–437, https://doi.org/10.1016/j.ensm.2019.04.022.
[7] J. Sun, H. Ye, J.A.S. Oh, Y. Sun, A. Plewa, Y. Wang, T. Wu, K. Zeng, L. Lu, Alleviating mechanical degradation of hexacyanoferrate via strain locking during Na^+ insertion/extraction for full sodium ion battery, Nano Res. 15 (2022) 2123–2129, https://doi.org/10.1007/s12274-021-3844-7.
[8] J. Sun, Q. Sun, H. Ye, Y. Wang, J.A.S. Oh, D. Ji, Q. Zeng, K. Zeng, L. Lu, Ammonium escorted chloride chemistry in stabilizing aqueous chloride ion battery, Mater. Today Energy 26 (2022) 101020, https://doi.org/10.1016/j.mtener.2022.101020.
[9] D. Sui, M. Yao, L. Si, K. Yan, J. Shi, J. Wang, C.C. Xu, Y. Zhang, Biomass-derived carbon coated SiO_2 nanotubes as superior anode for lithium-ion batteries, Carbon 205 (2023) 510–518, https://doi.org/10.1016/j.carbon.2023.01.039.
[10] J. Sun, H. Ye, J.A.S. Oh, A. Plewa, Y. Sun, T. Wu, Q. Sun, K. Zeng, L. Lu, Elevating the discharge plateau of prussian blue analogs through low-spin Fe redox induced intercalation pseudocapacitance, Energy Stor. Mater. 43 (2021) 182–189, https://doi.org/10.1016/j.ensm.2021.09.004.
[11] J. Sun, T. Wang, Y. Gao, Z. Pan, R. Hu, J. Wang, Will lithium-sulfur batteries be the next beyond-lithium ion batteries and even much better? InfoMat 4 (2022) e12359.
[12] L. Suo, O. Borodin, W. Sun, X. Fan, C. Yang, F. Wang, T. Gao, Z. Ma, M. Schroeder, A. von Cresce, S.M. Russell, M. Armand, A. Angell, K. Xu, C. Wang, Advanced high-voltage aqueous lithium-ion battery enabled by "Water-in-Bisalt" electrolyte, Angew. Chem. Int. Ed. 55 (2016) 7136–7141, https://doi.org/10.1002/anie.201602397.
[13] Y. Wang, L. Mu, J. Liu, Z. Yang, X. Yu, L. Gu, Y.-S. Hu, H. Li, X.-Q. Yang, L. Chen, X. Huang, A novel high capacity positive electrode material with tunnel-type structure for aqueous sodium-ion batteries, Adv. Energy Mater. 5 (2015) 1501005, https://doi.org/10.1002/aenm.201501005.
[14] L. Jiang, Y. Lu, C. Zhao, L. Liu, J. Zhang, Q. Zhang, X. Shen, J. Zhao, X. Yu, H. Li, X. Huang, L. Chen, Y.-S. Hu, Building aqueous K-ion batteries for energy storage, Nat. Energy 4 (2019) 495–503, https://doi.org/10.1038/s41560-019-0388-0.
[15] L. Chen, J.L. Bao, X. Dong, D.G. Truhlar, Y. Wang, C. Wang, Y. Xia, Aqueous Mg-Ion battery based on polyimide anode and prussian blue cathode, ACS Energy Lett. 2 (2017) 1115–1121, https://doi.org/10.1021/acsenergylett.7b00040.
[16] T.N. Vo, H. Kim, J. Hur, W. Choi, I.T. Kim, Surfactant-assisted ammonium vanadium oxide as a superior cathode for calcium-ion batteries, J. Mater. Chem. A 6 (2018) 22645–22654, https://doi.org/10.1039/C8TA07831A.
[17] Q. Zhao, M.J. Zachman, W.I. Al Sadat, J. Zheng, L.F. Kourkoutis, L. Archer, Solid electrolyte interphases for high-energy aqueous aluminum electrochemical cells, Sci. Adv. 4 (11) (2018).
[18] G. Liang, F. Mo, X. Ji, C. Zhi, Non-metallic charge carriers for aqueous batteries, Nat. Rev. Mater. 6 (2021) 109–123, https://doi.org/10.1038/s41578-020-00241-4.
[19] D. Chao, W. Zhou, F. Xie, C. Ye, H. Li, M. Jaroniec, S.-Z. Qiao, Roadmap for advanced aqueous batteries: from design of materials to applications, Sci. Adv. 6 (21) (2020).
[20] X. Wu, Y. Qi, J.J. Hong, Z. Li, A.S. Hernandez, X. Ji, Rocking-chair ammonium-ion battery: a highly reversible aqueous energy storage system, Angew. Chem. Int. Ed. 56 (2017) 13026–13030, https://doi.org/10.1002/anie.201707473.
[21] Y. Wang, S.F. Kuchena, Recent progress in aqueous ammonium-ion batteries, ACS Omega 7 (2022) 33732–33748, https://doi.org/10.1021/acsomega.2c04118.
[22] S.F. Kuchena, Y. Wang, V_2O_5 intercalated with polyaniline for improved kinetics in aqueous ammonium-ion batteries, Electrochim. Acta 425 (2022) 140751, https://doi.org/10.1016/j.electacta.2022.140751.
[23] Y. Wu, S. Dong, N. Lv, Z. Xu, R. Ren, G. Zhu, B. Huang, Y. Zhang, X. Dong, Unlocking the high capacity ammonium-ion storage in defective vanadium dioxide, Small 18 (2022) 2204888, https://doi.org/10.1002/smll.202204888.
[24] J. Han, A. Varzi, S. Passerini, The emergence of aqueous ammonium-ion batteries, Angew. Chem. Int. Ed. 61 (2022) e202115046.
[25] Z. Tian, V.S. Kale, Y. Wang, S. Kandambeth, J. Czaban-Jóźwiak, O. Shekhah, M. Eddaoudi, H.N. Alshareef, High-capacity NH_4^+ charge storage in covalent organic frameworks, J. Am. Chem. Soc. 143 (2021) 19178–19186, https://doi.org/10.1021/jacs.1c09290.

[26] Y. Song, Q. Pan, H. Lv, D. Yang, Z. Qin, M.-Y. Zhang, X. Sun, X.-X. Liu, Ammonium-ion storage using electrodeposited manganese oxides, Angew. Chem. Int. Ed. 60 (2021) 5718–5722, https://doi.org/10.1002/anie.202013110.

[27] D. Yu, Z. Wei, X. Zhang, Y. Zeng, C. Wang, G. Chen, Z.X. Shen, F. Du, Boosting Zn^{2+} and NH_4^+ storage in aqueous media via in-situ electrochemical induced VS_2/VO_x heterostructures, Adv. Funct. Mater. 31 (2021) 2008743, https://doi.org/10.1002/adfm.202008743.

[28] Q. Chen, J. Jin, M. Song, X. Zhang, H. Li, J. Zhang, G. Hou, Y. Tang, L. Mai, L. Zhou, High-energy aqueous ammonium-ion hybrid supercapacitors, Adv. Mater. 34 (2022) 2107992, https://doi.org/10.1002/adma.202107992.

[29] Y. An, Z. Li, Y. Sun, S. Li, Y. Xu, H. Dou, X. Zhang, Thermally chargeable ammonium-ion capacitor for energy storage and low-grade heat harvesting, Batteries Supercaps 5 (2022) e202200036.

[30] Z. Zhao, Y. Lei, L. Shi, Z. Tian, M.N. Hedhili, Y. Khan, H.N. Alshareef, A 2.75 V ammonium-based dual-ion battery, Angew. Chem. Int. Ed. 61 (2022) e202212941.

[31] Q. Pan, P. Hei, Y.u. Song, J. Meng, C. Liu, X.-X. Liu, Electrochemically activated nickel-cobalt double hydroxide for aqueous ammonium-zinc hybrid battery, Nano Res. 16 (2) (2023) 2495–2501.

[32] Y. Li, Y. Lu, C. Zhao, Y.-S. Hu, M.-M. Titirici, H. Li, X. Huang, L. Chen, Recent advances of electrode materials for low-cost sodium-ion batteries towards practical application for grid energy storage, Energy Stor. Mater. 7 (2017) 130–151, https://doi.org/10.1016/j.ensm.2017.01.002.

[33] W. Zheng, X. Hu, M. Wu, F. Zhan, Q. He, L. Chen, S. Chen, Advanced ammonium salt materials for electrochemical energy storage: recent progress and future perspectives, Chem. Eng. J. 454 (2023) 140194, https://doi.org/10.1016/j.cej.2022.140194.

[34] Z. Tian, J. Yin, T. Guo, Z. Zhao, Y. Zhu, Y. Wang, J. Yin, Y. Zou, Y. Lei, J. Ming, O. Bakr, O.F. Mohammed, H.N. Alshareef, A sustainable NH_4^+ ion battery by electrolyte engineering, Angew. Chem. Int. Ed. 61 (2022) e202213757.

[35] A. Eftekhari, Potassium secondary cell based on Prussian blue cathode, J. Power Sources 126 (2004) 221–228, https://doi.org/10.1016/j.jpowsour.2003.08.007.

[36] S. Qiu, Y. Xu, X. Wu, X. Ji, Prussian blue analogues as electrodes for aqueous monovalent ion batteries, Electrochem. Energy Rev. 5 (2022) 242–262, https://doi.org/10.1007/s41918-020-00088-x.

[37] X. Wu, Y. Ru, Y. Bai, G. Zhang, Y. Shi, H. Pang, PBA composites and their derivatives in energy and environmental applications, Coord. Chem. Rev. 451 (2022) 214260, https://doi.org/10.1016/j.ccr.2021.214260.

[38] K. Hurlbutt, S. Wheeler, I. Capone, M. Pasta, Prussian blue analogs as battery materials, Joule 2 (2018) 1950–1960, https://doi.org/10.1016/j.joule.2018.07.017.

[39] M. Xia, X. Zhang, H. Yu, Z. Yang, S. Chen, L. Zhang, M. Shui, Y. Xie, J. Shu, Hydrogen bond chemistry in $Fe_4[Fe(CN)_6]_3$ host for aqueous NH_4^+ batteries, Chem. Eng. J. 421 (2021) 127759, https://doi.org/10.1016/j.cej.2020.127759.

[40] G. Du, H. Pang, Recent advancements in Prussian blue analogues: Preparation and application in batteries, Energy Stor. Mater. 36 (2021) 387–408, https://doi.org/10.1016/j.ensm.2021.01.006.

[41] C. Li, W. Yan, S. Liang, P. Wang, J. Wang, L. Fu, Y. Zhu, Y. Chen, Y. Wu, W. Huang, Achieving a high-performance Prussian blue analogue cathode with an ultra-stable redox reaction for ammonium ion storage, Nanoscale Horiz. 4 (2019) 991–998, https://doi.org/10.1039/C8NH00484F.

[42] M. Wang, H. Zhang, J. Cui, S. Yao, X. Shen, T.J. Park, J.-K. Kim, Recent advances in emerging nonaqueous K-ion batteries: from mechanistic insights to practical applications, Energy Stor. Mater. 39 (2021) 305–346, https://doi.org/10.1016/j.ensm.2021.04.034.

[43] Y.-H. Zhu, X. Yang, T. Sun, S. Wang, Y.-L. Zhao, J.-M. Yan, X.-B. Zhang, Recent progresses and prospects of cathode materials for non-aqueous potassium-ion batteries, Electrochem. Energy Rev. 1 (2018) 548–566, https://doi.org/10.1007/s41918-018-0019-7.

[44] X. Wu, Y. Xu, H. Jiang, Z. Wei, J.J. Hong, A.S. Hernandez, F. Du, X. Ji, NH_4^+ Topotactic insertion in berlin green: an exceptionally long-cycling cathode in aqueous ammonium-ion batteries, ACS Appl. Energy Mater. 1 (2018) 3077–3083, https://doi.org/10.1021/acsaem.8b00789.

[45] W. Sun, F. Wang, S. Hou, C. Yang, X. Fan, Z. Ma, T. Gao, F. Han, R. Hu, M. Zhu, C. Wang, Zn/MnO_2 battery chemistry with H^+ and Zn^{2+} coinsertion, J. Am. Chem. Soc. 139 (2017) 9775–9778, https://doi.org/10.1021/jacs.7b04471.

[46] S. Li, M. Xia, C. Xiao, X. Zhang, H. Yu, L. Zhang, J. Shu, Common ion effect enhanced Prussian blue analogues for aqueous ammonium ion storage, Dalton Trans. 50 (2021) 6520–6527, https://doi.org/10.1039/D1DT00805F.

[47] Y. Li, J. Zhao, Q. Hu, T. Hao, H. Cao, X. Huang, Y. Liu, Y. Zhang, D. Lin, Y. Tang, Y. Cai, Prussian blue analogs cathodes for aqueous zinc ion batteries, Mater. Today Energy 29 (2022) 101095, https://doi.org/10.1016/j.mtener.2022.101095.

[48] Z. Li, T. Liu, R. Meng, L. Gao, Y. Zou, P. Peng, Y. Shao, X. Liang, Insights into the structure stability of Prussian blue for aqueous zinc ion batteries, Energy Environ. Mater. 4 (2021) 111–116, https://doi.org/10.1002/eem2.12108.

[49] C.D. Wessells, S.V. Peddada, M.T. McDowell, R.A. Huggins, Y.i. Cui, The effect of insertion species on nanostructured open framework hexacyanoferrate battery electrodes, J. Electrochem. Soc. 159 (2) (2011) A98–A103.

[50] H. Yu, J. Xu, C. Deng, M. Xia, X. Zhang, J. Shu, Z. Wang, The nature of the ultrahigh initial coulombic efficiency of $Ni_2Fe(CN)_6$ in aqueous ammonium-ion batteries, ACS Appl. Energy Mater. 4 (2021) 9594–9599, https://doi.org/10.1021/acsaem.1c01725.

[51] H. Yu, L. Fan, H. Yan, C. Deng, L. Yan, J. Shu, Z.-B. Wang, Nickel ferrocyanides for aqueous ammonium ion batteries, Inorg. Chem. Front. 9 (2022) 2001–2010, https://doi.org/10.1039/D2QI00265E.

[52] H. Yu, L. Fan, H. Yan, C. Deng, L. Yan, J. Shu, Z.-B. Wang, Optimizing NH_4^+ storage capability of nickel ferrocyanide by regulating coordination anion in aqueous electrolytes, ChemElectroChem 9 (2022) e202200492.

[53] H. Yu, L. Fan, C. Deng, H. Yan, L. Yan, J. Shu, Z.-B. Wang, Enabling nickel ferrocyanide nanoparticles for high-performance ammonium ion storage, Front. Chem. Sci. Eng. 17 (2) (2023) 226–235.

[54] L. Yan, Y.-e. Qi, X. Dong, Y. Wang, Y. Xia, Ammonium-ion batteries with a wide operating temperature window from −40 to 80°C, eScience 1 (2) (2021) 212–218.

[55] W. Hou, C. Yan, P. Shao, K. Dai, J. Yang, Interface and electronic structure engineering induced Prussian blue analogues with ultra-stable capability for aqueous NH_4^+ storage, Nanoscale 14 (2022) 8501–8509, https://doi.org/10.1039/D2NR01735K.

[56] X. Zhang, M. Xia, T. Liu, N. Peng, H. Yu, R. Zheng, L. Zhang, M. Shui, J. Shu, Copper hexacyanoferrate as ultra-high rate host for aqueous ammonium ion storage, Chem. Eng. J. 421 (2021) 127767, https://doi.org/10.1016/j.cej.2020.127767.

[57] X. Zhang, M. Xia, H. Yu, J. Zhang, Z. Yang, L. Zhang, J. Shu, Hydrogen bond-assisted ultra-stable and fast aqueous NH_4^+ storage, Nano-Micro Lett. 13 (2021) 139, https://doi.org/10.1007/s40820-021-00671-x.

[58] J. Han, M. Zarrabeitia, A. Mariani, M. Kuenzel, A. Mullaliu, A. Varzi, S. Passerini, Concentrated electrolytes enabling stable aqueous ammonium-ion batteries, Adv. Mater. 34 (2022) 2201877, https://doi.org/10.1002/adma.202201877.

[59] J.-H. Lee, G. Ali, D.H. Kim, K.Y. Chung, Metal-organic framework cathodes based on a vanadium hexacyanoferrate Prussian blue analogue for high-performance aqueous rechargeable batteries, Adv. Energy Mater. 7 (2017) 1601491, https://doi.org/10.1002/aenm.201601491.

[60] J. Xing, X. Fu, S. Guan, Y. Zhang, M. Lei, Z. Peng, Novel K-V-Fe Prussian blue analogues nanocubes for high-performance aqueous ammonium ion batteries, Appl. Surf. Sci. 543 (2021) 148843, https://doi.org/10.1016/j.apsusc.2020.148843.

[61] H. Zhang, Y. Tian, W. Wang, Z. Jian, W. Chen, Organic Ammonium ion battery: a new strategy for a nonmetallic ion energy storage system, Angew. Chem. Int. Ed. 61 (2022) e202204351.

[62] L. Du, S. Bi, M. Yang, Z. Tie, M. Zhang, Z. Niu, Coupling dual metal active sites and low-solvation architecture toward high-performance aqueous ammonium-ion batteries, e2214545119, Proc. Natl. Acad. Sci. 119 (2022), https://doi.org/10.1073/pnas.2214545119.

[63] T.-F. Yi, L. Qiu, J.-P. Qu, H. Liu, J.-H. Zhang, Y.-R. Zhu, Towards high-performance cathodes: design and energy storage mechanism of vanadium oxides-based materials for aqueous Zn-ion batteries, Coord. Chem. Rev. 446 (2021) 214124, https://doi.org/10.1016/j.ccr.2021.214124.

[64] Y. Zhu, Z. Zhang, J. Bao, S. Zeng, W. Nie, P. Chen, Y. Zhou, Y. Xu, Multi-metal doped high capacity and stable Prussian blue analogue for sodium ion batteries, Int. J. Energ. Res. 44 (2020) 9205–9212, https://doi.org/10.1002/er.5576.

[65] S. Dong, W. Shin, H. Jiang, X. Wu, Z. Li, J. Holoubek, W.F. Stickle, B. Key, C. Liu, J. Lu, P.A. Greaney, X. Zhang, X. Ji, Ultra-fast NH_4^+ storage: strong H bonding between NH_4^+ and Bi-layered V_2O_5, Chemistry 5 (2019) 1537–1551, https://doi.org/10.1016/j.chempr.2019.03.009.

[66] X. Xu, M. Duan, Y. Yue, Q.i. Li, X. Zhang, L.u. Wu, P. Wu, B.o. Song, L. Mai, Bilayered $Mg_{0.25}V_2O_5{\cdot}H_2O$ as a stable cathode for rechargeable Ca-ion batteries, ACS Energy Lett. 4 (6) (2019) 1328–1335.

[67] Y. Xu, X. Deng, Q. Li, G. Zhang, F. Xiong, S. Tan, Q. Wei, J. Lu, J. Li, Q. An, L. Mai, Vanadium oxide pillared by interlayer Mg^{2+} ions and water as ultralong-life cathodes for magnesium-ion batteries, Chemistry 5 (2019) 1194–1209, https://doi.org/10.1016/j.chempr.2019.02.014.

[68] C. Han, J. Zhu, K. Fu, D. Deng, W. Luo, L. Mai, A high-capacity polyaniline-intercalated layered vanadium oxide for aqueous ammonium-ion batteries, Chem. Commun. 58 (2022) 791–794, https://doi.org/10.1039/D1CC05677H.

[69] L. Xing, H. Chen, X. Wen, W. Zhou, K. Xiang, High performance of co-doped V_2O_5 cathode material in V_2O_5-saturated $(NH_4)_2SO_4$ electrolyte for ammonium ion battery, J. Alloys Compd. 925 (2022) 166652, https://doi.org/10.1016/j.jallcom.2022.166652.

[70] J. Sun, W. Nie, S. Xu, P. Gao, S. Sun, X. Zheng, Q. Hu, Z. Xu, in: Polymers, 2022.

[71] H. Li, J. Yang, J. Cheng, T. He, B. Wang, Flexible aqueous ammonium-ion full cell with high rate capability and long cycle life, Nano Energy 68 (2020) 104369, https://doi.org/10.1016/j.nanoen.2019.104369.

[72] S. Farai Kuchena, Y. Wang, A full flexible NH_4^+ ion battery based on the concentrated hydrogel electrolyte for enhanced performance, Chem. Eur. J. 27 (2021) 15450–15459, https://doi.org/10.1002/chem.202102442.

[73] W. Xu, L. Zhang, K. Zhao, X. Sun, Q. Wu, Layered ferric vanadate nanosheets as a high-rate NH_4^+ storage electrode, Electrochim. Acta 360 (2020) 137008, https://doi.org/10.1016/j.electacta.2020.137008.

[74] H. Li, W. Zhang, K. Sun, J. Guo, K. Yuan, J. Fu, T. Zhang, X. Zhang, H. Long, Z. Zhang, Y. Lai, H. Sun, Manganese-based materials for rechargeable batteries beyond lithium-ion, Adv. Energy Mater. 11 (2021) 2100867, https://doi.org/10.1002/aenm.202100867.

[75] Y. Gao, H. Yang, Y. Bai, C. Wu, Mn-based oxides for aqueous rechargeable metal ion batteries, J. Mater. Chem. A 9 (2021) 11472–11500, https://doi.org/10.1039/D1TA01951A.

[76] W. Shi, W.S.V. Lee, J. Xue, Recent development of Mn-based oxides as zinc-ion battery cathode, ChemSusChem 14 (2021) 1634–1658, https://doi.org/10.1002/cssc.202002493.

[77] N. Wang, J. Ma, Z. Liu, J. Xu, D. Zhao, N. Wang, C. Yang, Y. Cao, J. Lu, J. Zhang, An air-stable iron/manganese-based phosphate cathode for high performance

sodium-ion batteries, Chem. Eng. J. 433 (2022) 133798, https://doi.org/10.1016/j.cej.2021.133798.
[78] D. Yang, Y. Song, M.-Y. Zhang, Z. Qin, J. Liu, X.-X. Liu, Solid-liquid interfacial coordination chemistry enables high-capacity ammonium storage in amorphous manganese phosphate, Angew. Chem. Int. Ed. 61 (2022) e202207711.
[79] S.F. Kuchena, Y. Wang, Superior polyaniline cathode material with enhanced capacity for ammonium ion storage, ACS Appl. Energy Mater. 3 (2020) 11690–11698, https://doi.org/10.1021/acsaem.0c01791.
[80] J.J. Shea, C. Luo, Organic electrode materials for metal ion batteries, ACS Appl. Mater. Interfaces 12 (2020) 5361–5380, https://doi.org/10.1021/acsami.9b20384.
[81] Z. Zhao, T. Yu, Y. Miao, X. Zhao, Chloride ion-doped polyaniline/carbon nanotube nanocomposite materials as new cathodes for chloride ion battery, Electrochim. Acta 270 (2018) 30–36, https://doi.org/10.1016/j.electacta.2018.03.077.
[82] J. Deng, X. Wang, J. Guo, P. Liu, Effect of the oxidant/monomer ratio and the washing post-treatment on electrochemical properties of conductive polymers, Ind. Eng. Chem. Res. 53 (2014) 13680–13689, https://doi.org/10.1021/ie501366x.
[83] W. Deng, Y. Shen, J. Qian, Y. Cao, H. Yang, A perylene diimide crystal with high capacity and stable cyclability for Na-Ion batteries, ACS Appl. Mater. Interfaces 7 (2015) 21095–21099, https://doi.org/10.1021/acsami.5b04325.
[84] D. Wu, F. Jing, X. Xi, L. Ma, D. Lu, P. Yang, R. Liu, An acid-pasting approach towards perylenetetracarboxylic diimide based lithium/sodium ion battery cathodes with high rate performances, J. Colloid Interface Sci. 538 (2019) 597–604, https://doi.org/10.1016/j.jcis.2018.11.085.
[85] Y. Bai, W. Fu, W. Chen, Z. Chen, X. Pan, X. Lv, J. Wu, X. Pan, Perylenetetracarboxylic diimide as a high-rate anode for potassium-ion batteries, J. Mater. Chem. A 7 (2019) 24454–24461, https://doi.org/10.1039/C9TA07605K.
[86] Z. Song, H. Zhan, Y. Zhou, Polyimides: promising energy-storage materials, Angew. Chem. Int. Ed. 49 (2010) 8444–8448, https://doi.org/10.1002/anie.201002439.
[87] S. Qiu, Y. Xu, X. Li, S.K. Sandstrom, X. Wu, X. Ji, Reinforced potassium and ammonium storage of the polyimide anode in acetate-based water-in-salt electrolytes, Electrochem. Commun. 122 (2021) 106880, https://doi.org/10.1016/j.elecom.2020.106880.
[88] X. Chen, Y. Li, L. Wang, Y. Xu, A. Nie, Q. Li, F. Wu, W. Sun, X. Zhang, R. Vajtai, P. M. Ajayan, L. Chen, Y. Wang, High-lithium-affinity chemically exfoliated 2D covalent organic frameworks, Adv. Mater. 31 (2019) 1901640, https://doi.org/10.1002/adma.201901640.
[89] L. Zhong, Y. Lu, H. Li, Z. Tao, J. Chen, High-performance aqueous sodium-ion batteries with hydrogel electrolyte and alloxazine/CMK-3 anode, ACS Sustain. Chem. Eng. 6 (2018) 7761–7768, https://doi.org/10.1021/acssuschemeng.8b00663.
[90] Y. Ma, T. Sun, Q. Nian, S. Zheng, T. Ma, Q. Wang, H. Du, Z. Tao, Alloxazine as anode material for high-performance aqueous ammonium-ion battery, Nano Res. 15 (2022) 2047–2051, https://doi.org/10.1007/s12274-021-3777-1.
[91] S. Yuan, X. Duan, J. Liu, Y. Ye, F. Lv, T. Liu, Q. Wang, X. Zhang, Recent progress on transition metal oxides as advanced materials for energy conversion and storage, Energy Stor. Mater. 42 (2021) 317–369, https://doi.org/10.1016/j.ensm.2021.07.007.
[92] J.J. Holoubek, H. Jiang, D. Leonard, Y. Qi, G.C. Bustamante, X. Ji, Amorphous titanic acid electrode: its electrochemical storage of ammonium in a new water-in-salt electrolyte, Chem. Commun. 54 (2018) 9805–9808, https://doi.org/10.1039/C8CC04713H.
[93] J. Xie, H. Zhang, Q. Liu, X. Liu, X. Lu, Recent progress of molybdenum-based materials in aqueous rechargeable batteries, Mater. Today Adv. 8 (2020) 100100, https://doi.org/10.1016/j.mtadv.2020.100100.
[94] G. Liang, Y. Wang, Z. Huang, F. Mo, X. Li, Q. Yang, D. Wang, H. Li, S. Chen, C. Zhi, Initiating hexagonal MoO_3 for superb-stable and fast NH_4^+ storage based on hydrogen bond chemistry, Adv. Mater. 32 (2020) 1907802, https://doi.org/10.1002/adma.201907802.
[95] Y.-Z. Zhang, J. Liang, Z. Huang, Q. Wang, G. Zhu, S. Dong, H. Liang, X. Dong, Ionically conductive tunnels in h-WO_3 enable high-rate NH_4^+ storage, Adv. Sci. 9 (2022) 2105158, https://doi.org/10.1002/advs.202105158.
[96] X. Mu, Y. Song, Z. Qin, J. Meng, Z. Wang, X.-X. Liu, Core-shell structural vanadium Oxide/Polypyrrole anode for aqueous Ammonium-Ion batteries, Chem. Eng. J. 453 (2023) 139575, https://doi.org/10.1016/j.cej.2022.139575.
[97] J. Come, M. Naguib, P. Rozier, M.W. Barsoum, Y. Gogotsi, P.-L. Taberna, M. Morcrette, P. Simon, A non-aqueous asymmetric cell with a Ti_2C-based two-dimensional negative electrode, J. Electrochem. Soc. 159 (8) (2012) A1368–A1373.
[98] X. Xu, W. Liu, Y. Kim, J. Cho, Nanostructured transition metal sulfides for lithium ion batteries: progress and challenges, Nano Today 9 (2014) 604–630, https://doi.org/10.1016/j.nantod.2014.09.005.
[99] M.R. Lukatskaya, O. Mashtalir, C.E. Ren, Y. Dall'Agnese, P. Rozier, P.L. Taberna, M. Naguib, P. Simon, M.W. Barsoum, Y. Gogotsi, Cation intercalation and high volumetric capacitance of two-dimensional titanium carbide, Science 341 (6153) (2013) 1502–1505.
[100] M. Xie, W. Zhao, Y. Mao, F. Huang, $K_{0.38}(H_2O)_{0.82}MoS_2$ as a universal host for rechargeable aqueous cation (K^+, Na^+, Li^+, NH_4^+, Mg^{2+}, Al^{3+}) batteries, Dalton Trans. 49 (2020) 3488–3494, https://doi.org/10.1039/D0DT00471E.
[101] P. Wang, Y. Zhang, H. Jiang, X. Dong, C. Meng, Ammonium vanadium oxide framework with stable NH_4^+ aqueous storage for flexible quasi-solid-state supercapacitor, Chem. Eng. J. 427 (2022) 131548, https://doi.org/10.1016/j.cej.2021.131548.
[102] X. Chen, P. Wang, Z. Feng, C. Meng, Y. Zhang, Conductive polymer intercalated vanadium oxide on carbon cloth for fast ammonium-ion storage in supercapacitor applications, Chem. Eng. J. 445 (2022) 136747, https://doi.org/10.1016/j.cej.2022.136747.
[103] X. Chen, P. Wang, Z. Feng, Y. Liu, M. Cui, C. Meng, Y. Zhang, Structural regulation of vanadium oxide by poly(3,4-ethylenedioxithiophene) intercalation for ammonium-ion supercapacitors, Adv. Sens. Energy Mater. 1 (2) (2022) 100013, https://doi.org/10.1016/j.asems.2022.100013.
[104] S. Kumar, G. Saeed, L. Zhu, K.N. Hui, N.H. Kim, J.H. Lee, 0D to 3D carbon-based networks combined with pseudocapacitive electrode material for high energy density supercapacitor: a review, Chem. Eng. J. 403 (2021) 126352, https://doi.org/10.1016/j.cej.2020.126352.
[105] C. Choi, D.S. Ashby, D.M. Butts, R.H. DeBlock, Q. Wei, J. Lau, B. Dunn, Achieving high energy density and high power density with pseudocapacitive materials, Nat. Rev. Mater. 5 (2020) 5–19, https://doi.org/10.1038/s41578-019-0142-z.
[106] P. Wang, Y. Zhang, Z. Feng, Y. Liu, C. Meng, A dual-polymer strategy boosts hydrated vanadium oxide for ammonium-ion storage, J. Colloid Interface Sci. 606 (2022) 1322–1332, https://doi.org/10.1016/j.jcis.2021.08.036.
[107] K.C.S. Lakshmi, X. Ji, T.-Y. Chen, B. Vedhanarayanan, T.-w. Lin, Pseudocapacitive and battery-type organic polymer electrodes for a 1.9 V hybrid supercapacitor with a record concentration of ammonium acetate, J. Power Sources 511 (2021) 230434, https://doi.org/10.1016/j.jpowsour.2021.230434.
[108] D. Wang, L. Wang, G. Liang, H. Li, Z. Liu, Z. Tang, J. Liang, C. Zhi, A superior δ-MnO_2 cathode and a self-healing Zn-δ-MnO_2 battery, ACS Nano 13 (2019) 10643–10652, https://doi.org/10.1021/acsnano.9b04916.
[109] J. Chen, W. Xu, H. Wang, X. Ren, F. Zhan, Q. He, H. Wang, L. Chen, Emerging two-dimensional nanostructured manganese-based materials for electrochemical energy storage: recent advances, mechanisms, challenges, and prospects, J. Mater. Chem. A 10 (2022) 21197–21250, https://doi.org/10.1039/D2TA05309H.
[110] K.C. Seetha Lakshmi, X. Ji, L.-D. Shao, B. Vedhanarayanan, T.-W. Lin, Tailor-made organic polymers towards high voltage aqueous ammonium/potassium-ion asymmetric supercapacitors, Appl. Surf. Sci. 577 (2022) 151918, https://doi.org/10.1016/j.apsusc.2021.151918.
[111] Q. Chen, M. Song, X. Zhang, J. Zhang, G. Hou, Y. Tang, Ammonium ion pre-intercalation stabilized tunnel h-WO_3 for fast NH_4^+ storage, J. Mater. Chem. A 10 (2022) 15614–15622, https://doi.org/10.1039/D2TA03643F.
[112] J. Dai, X. Qi, L. Xia, Q. Xue, L. Luo, X. Wang, C. Yang, D. Li, H. Xie, A. Cabot, L. Dai, Y. Xu, Aqueous ammonium-ion supercapacitors with unprecedented energy density and stability enabled by oxygen vacancy-enriched MoO_3@C, Adv. Funct. Mater. n/a (2022) 2212440, https://doi.org/10.1002/adfm.202212440.
[113] L. Han, J. Luo, R. Zhang, W. Gong, L. Chen, F. Liu, Y. Ling, Y. Dong, Z. Yong, Y. Zhang, L. Wei, X. Zhang, Q. Zhang, Q. Li, Arrayed heterostructures of MoS_2 nanosheets anchored TiN nanowires as efficient pseudocapacitive anodes for fiber-shaped ammonium-ion asymmetric supercapacitors, ACS Nano 16 (2022) 14951–14962, https://doi.org/10.1021/acsnano.2c05905.
[114] C. Lin, Y. Wang, F. Zhong, H. Yu, Y. Yan, S. Wu, Carbon materials for high-performance potassium-ion energy-storage devices, Chem. Eng. J. 407 (2021) 126991, https://doi.org/10.1016/j.cej.2020.126991.
[115] A. Jagadale, X. Zhou, R. Xiong, D.P. Dubal, J. Xu, S. Yang, Lithium ion capacitors (LICs): development of the materials, Energy Stor. Mater. 19 (2019) 314–329, https://doi.org/10.1016/j.ensm.2019.02.031.
[116] H. Chen, C. Dai, Y. Li, R. Zhan, M.-Q. Wang, B. Guo, Y. Zhang, H. Liu, M. Xu, S.-J. Bao, An excellent full sodium-ion capacitor derived from a single Ti-based metal–organic framework, J. Mater. Chem. A 6 (2018) 24860–24868, https://doi.org/10.1039/C8TA09072F.
[117] Y. Zhang, Y. An, B. Yin, J. Jiang, S. Dong, H. Dou, X. Zhang, A novel aqueous ammonium dual-ion battery based on organic polymers, J. Mater. Chem. A 7 (2019) 11314–11320, https://doi.org/10.1039/C9TA00254E.
[118] G. Zhou, X. An, C. Zhou, Y. Wu, Y.-E. Miao, T. Liu, Highly porous electroactive polyimide-based nanofibrous composite anode for all-organic aqueous ammonium dual-ion batteries, Compos. Commun. 22 (2020) 100519, https://doi.org/10.1016/j.coco.2020.100519.
[119] R. Zheng, Y. Li, H. Yu, X. Zhang, D. Yang, L. Yan, Y. Li, J. Shu, B.-L. Su, Ammonium ion batteries: material, electrochemistry and strategy, Angew. Chem. Int. Ed. n/a (2023) e202301629.
[120] C. Li, D. Zhang, F. Ma, T. Ma, J. Wang, Y. Chen, Y. Zhu, L. Fu, Y. Wu, W. Huang, A high-rate and long-life aqueous rechargeable ammonium zinc hybrid battery, ChemSusChem 12 (2019) 3732–3736, https://doi.org/10.1002/cssc.201901622.
[121] C. Li, J. Wu, F. Ma, Y. Chen, L. Fu, Y. Zhu, Y. Zhang, P. Wang, Y. Wu, W. Huang, High-rate and high-voltage aqueous rechargeable zinc ammonium hybrid battery from selective cation intercalation cathode, ACS Appl. Energy Mater. 2 (2019) 6984–6989, https://doi.org/10.1021/acsaem.9b01469.